Journal of Controlled Release 357 (2023) 67–83

Contents lists available at ScienceDirect

Journal of Controlled Release

journal homepage: www.elsevier.com/locate/jconrel

Targeted siRNA lipid nanoparticles for the treatment of KRAS-mutant tumors

Shubaash Anthiya [a], Süleyman Can Öztürk [c], Hamdullah Yanik [d], Ece Tavukcuoglu [d], Adem Şahin [e], Dhrubajyoti Datta [f], Klaus Charisse [f], David Moreira Álvarez [g], María Isabel Loza [g], Alfonso Calvo [h,i], Einar Sulheim [j], Simon Loevenich [j], Geir Klinkenberg [j], Ruth Schmid [j], Muthiah Manoharan [f], Güneş Esendağlı [d], Maria Jose Alonso [a,b,*]

[a] Center for Research in Molecular Medicine and Chronic Diseases (CIMUS), Universidade de Santiago de Compostela, Santiago de Compostela 15782, Spain
[b] Department of Pharmacology Pharmacy and Pharmaceutical Technology, School of Pharmacy, Universidade de Santiago de Compostela, Santiago de Compostela 15782, Spain
[c] Research and Application Center for Animal Experiments, Hacettepe University Cancer Institute, Ankara, Turkey
[d] Department of Basic Oncology, Hacettepe University Cancer Institute, Ankara, Turkey
[e] R&D Department of ILKO Pharmaceuticals, Ankara, Turkey
[f] Alnylam Pharmaceuticals, 675 West Kendall, Cambridge, MA 02142, United States
[g] BioFarma Research Group, CIMUS, Universidade de Santiago de Compostela, Santiago de Compostela, Spain
[h] Health Research Institute of Navarra (IDISNA), Pamplona, Spain
[i] Department of Histology and Pathology, School of Medicine, University of Navarra, Pamplona, Spain
[j] Department of Biotechnology and Nanomedicine, SINTEF Industry, Trondheim, Norway

ARTICLE INFO

Keywords:
RNA therapeutics
siRNA
Targeted delivery
LNPs
KRAS
Combination therapy
Pancreatic cancer

ABSTRACT

K-RAS is a highly relevant oncogene that is mutated in approximately 90% of pancreatic cancers and 20–25% of lung adenocarcinomas. The aim of this work was to develop a new anti-KRAS siRNA therapeutic strategy through the engineering of functionalized lipid nanoparticles (LNPs). To do this, first, a potent pan anti-KRAS siRNA sequence was chosen from the literature and different chemical modifications of siRNA were tested for their transfection efficacy (KRAS knockdown) and anti-proliferative effects on various cancer cell lines. Second, a selected siRNA candidate was loaded into tLyp-1 targeted and non-targeted lipid nanoparticles (LNPs). The biodistribution and antitumoral efficacy of selected siRNA-loaded LNP-prototypes were evaluated *in vivo* using a pancreatic cancer murine model (subcutaneous xenograft CFPAC-1 tumors). Our results show that tLyp-1-tagged targeted LNPs have an enhanced accumulation in the tumor compared to non-targeted LNPs. Moreover, a significant reduction in the pancreatic tumor growth was observed when the anti-KRAS siRNA treatment was combined with a classical chemotherapeutic agent, gemcitabine. In conclusion, our work demonstrates the benefits of using a targeting approach to improve tumor accumulation of siRNA-LNPs and its positive impact on tumor reduction.

1. Introduction

KRAS (Kirsten rat sarcoma viral oncogene homolog) oncoprotein is a clinically relevant target in cancer therapy [1]. Indeed, KRAS mutations are found in approximately 90% of pancreatic cancers [2], 20–25% of lung adenocarcinomas [3] and, also, in other types of cancer. Mutant KRAS promotes cancer growth, immune suppression, and remodels the tumor microenvironment by secreting various cytokines, chemokines, and growth factors [2]. The KRAS mutation most frequently occurs either at the codon for Glycine-12 (G12) or Glycine-13 (G13) [3]. Interestingly, so far, the KRAS mutations, with the exception of the G12C mutation, have been identified as undruggable targets when using small molecule inhibitors [2]. Hence, in our view, the design of a siRNA-based approach to silence the KRAS expression may represent a very attractive and valuable therapeutic strategy [1,4].

Two different anti-KRAS siRNA designs have been reported,

* Corresponding author at: Center for Research in Molecular Medicine and Chronic Diseases (CIMUS), Universidade de Santiago de Compostela, Santiago de Compostela 15782, Spain.
E-mail address: mariaj.alonso@usc.es (M.J. Alonso).

https://doi.org/10.1016/j.jconrel.2023.03.016
Received 1 November 2022; Received in revised form 12 February 2023; Accepted 9 March 2023
Available online 28 March 2023

targeting either a specific KRAS mutation [4–13] or all KRAS mutations (pan-KRAS) [1,14–17]. Both mutation-specific anti-KRAS siRNA and pan-KRAS siRNA or antisense oligonucleotide treatments have been reported to selectively kill tumors that are dependent on the KRAS-mutation for survival [1,4–17] without eliciting significant toxicity [1,16–19].

In this work, we selected a pan-KRAS siRNA sequence based on a previous study that showed >80% silencing at very low doses (0.1–2 nM concentration) with the least off-target effects [1]. Based on previous knowledge about the potential of chemical modifications to improve siRNA stability, silencing efficacy, long-term activity and reduced non-specific immune activation [20–22], three different chemically stabilized siRNAs were designed and compared with the unmodified siKRAS regarding their *in vitro* KRAS silencing and anti-cancer activity. Then, we selected the two siRNAs that showed the most promise and formulated one of them into appropriate delivery carriers.

According to the literature, an array of delivery carriers has been proposed for the delivery of siRNA anti-KRAS. Among them, PLGA-siRNA implants for local delivery [4,8,9,23], and polymer nanoparticles and assemblies [1,13,14,16], liposomes [6,10,15], exosomes (iExosomes) [10], and melittin-based peptide delivery systems [17] for systemic administration of anti-KRAS siRNA has been reported. Some of these strategies, such as long circulating iExosomes (NCT03608631) and PLGA-siRNA implants (NCT01676259), are currently under clinical development [9]. Additionally, identifying a suitable combination therapy is critical to improve the anti-KRAS siRNA treatment outcome [1,6,14,16]. All in all, there has been a significant progress in terms of understanding the role of KRAS in the treatment of cancer, and in the development of nanotechnology tools for the *in vivo* delivery of siRNA [23]. However, site-specific delivery of siRNA to the tumors while avoiding its accumulation in off-target organs, such as liver, is a major challenge that still needs to be overcome.

Lipid nanoparticles (LNPs) are the most efficient and clinically proven delivery systems for siRNA and messenger RNAs [22,24,25]. Currently, the clinical application of LNPs is limited to the treatment of liver diseases and vaccine delivery due to the prominent accumulation and functional delivery of RNA cargo to the liver and at the site of injection following a parenteral route of administration [22–28]. To achieve functional delivery of RNA-LNPs to other organs, several strategies have been explored, such as the optimization of the lipids composition [26–32], the modulation of the ratio between the cationic and the negative charges of the lipids and RNA, respectively [33], the introduction of targeting ligands [34,35], as well as the modulation of the protein corona [30,31] and the saturation of the liver uptake [36,37]. Our lab and others have found that, among the tumor targeting ligands, truncated Lyp-1 (tLyp-1) has good vascular permeation and tumor homing properties [38–40]. In fact, we have previously reported an excellent tumor accumulation and therapeutic efficacy when docetaxel was formulated into tLyp-1-functionalized nanocapsules [39].

Based on this previous knowledge, in this work, a potent pan anti-KRAS siRNA sequence was chosen from the literature and different chemical modifications of siRNA were tested for their *in vitro* transfection efficacy (KRAS knockdown, phosphoERK down-regulation) and anti-proliferative effects on various cancer cell lines. Then, the selected siRNA candidate was loaded into tLyp-1 targeted and non-targeted lipid nanoparticles (LNPs). The biodistribution and antitumoral efficacy of the most promising candidate was evaluated *in vivo* using a pancreatic cancer murine model (subcutaneous xenograft CFPAC-1 tumors), while the toxicity was evaluated in a healthy mouse model.

2. Materials and methods

2.1. Materials

siTTR-ESC+, siKRAS-ESC+, siKRAS-LNA, siKRAS-Chol, 1,1′-((2-(4-(2-((2-(bis(2-hydroxydodecyl)amino)ethyl)(2-hydroxydodecyl)amino) ethyl)piperazin-1-yl)ethyl)azanediyl)bis(dodecan-2-ol) (C12–200, HCl salt), and (*R*)-methoxy-polyethyleneglycol-2000-carbamoyl-di-O-myristyl-sn-glyceride (DMG-PEG2000) were a generous gift from Alnylam Pharmaceuticals, Cambridge, USA. siRNAs without special chemical modifications, siGFP and siKRAS-Unmod, were purchased from Bio-Spring GmbH, Germany. The siRNA sequences are presented in Table 1, while the schematic design of siKRAS and the structure of chemical modifications are presented in Fig. 2. The ionizable lipid 3,6-bis[4-[bis (2-hydroxydodecyl)amino]butyl]-2,5-piperazinedione (cKK-E12) was a generous gift from Prof. Daniel G. Anderson from Massachusetts Institute of Technology, Cambridge, USA. 1,2-dioleoyl-3-trimethylammonium-propane (chloride salt) (DOTAP), 1,2-dioleoyl-sn-glycero-3-phosphoethanolamine (DOPE) and 1,2-distearoyl-sn-glycero-3-phosphoethanolamine-N-[maleimide(polyethylene glycol)-2000] (ammonium salt) (DSPE-PEG2000-Maleimide, or DPM) were purchased from Avanti Polar Lipids, USA. Cholesterol was purchased from Sigma Aldrich, USA. Polysorbate-80 (Tween® 80) was purchased from Merck Millipore. INTERFERin® was purchased from Polyplus-transfection® SA, France. Florescent dyes, DiD (1,1'-Dioctadecyl-3,3,3′,3'-Tetramethylindodicarbocyanine, 4-Chlorobenzenesulfonate Salt) and DiR (1,1'-Dioctadecyl-3,3,3′,3'-Tetramethylindotricarbocyanine Iodide), were purchased from Invitrogen, Thermo Fisher Scientific. Truncated Lyp-1 peptide (tLyp-1, CGNKRTR, 97% purity) was purchased from China peptides. The structure of LNPs and their component lipids are presented in Fig. 1.

2.2. LNP formulation details

2.2.1. Preparation of siRNA loaded cationic lipid nanoparticles (cLNPs) (RNA adsorbed)

DOTAP-based cationic lipid nanoparticles (cLNPs) were prepared with cholesterol and Tween® 80 in the presence of a fusogenic lipid DOPE. The blank cLNPs were prepared by mixing an ethanol phase containing component lipids and an aqueous phase containing water under magnetic stirring. In a second step, an siRNA solution (100 μL, 0.2

Table 1
Details of siRNAs used in this work.

Entry	Name	Strand	Sequence (5′ – 3 ′)
I	siPan-KRAS#1	antisense	UGAAUUAGCUGUAUCGUCAAGdTdT
		sense	CUUGACGAUACAGCUAAUUCAdTdT
II	siPan-KRAS#2	antisense	ACUGUACUCCUCUUGACCUGdTdT
		sense	CAGGUCAAGAGGAGUACAGUdTdT
III	siKRAS #1 (#1)	antisense	GUGCAAUGAGGGACCAGUAdTdT
		sense	UACUGGUCCCUCAUUGCACdTdT
IV	siKRAS #2 (#2)	antisense	CUUAGAAAAAAGAAGGUUUCCdTdT
		sense	GGAAACCUUCUUUUUUCUAAGdTdT
V	siKRAS-Unmod	antisense	P-UGAAUUAGCUGUAUCGUCGAC
		sense	CGACGAUACAGCUAAUUCAUA
VI	siKRAS-ESC+	antisense	VP-u●*G*●a*Au**Ua**Gc**U*gua*Uc**Gu**Ca**Ag*●g●c
		sense	c●u●*Ug**Ac**Ga**UA**Ca**Gc**Ua**Au**U*●c●a
VII	siKRAS-LNA	antisense	VP-u●*G*●a*Au**Ua**Gc**U*gua*Uc**Gu**Ca**Ag*●g●c
		sense	m5C^{L}●T^{L}●*Ug**Ac**Ga**UA**Ca**Gc**Ua**Au**U*●c●a
VIII	siKRAS-Chol	antisense	VP-u●*G*●a*Au**Ua**Gc**U*gua*Uc**Gu**Ca**Ag*●g●c
		sense	c●u●*Ug**Ac**Ga**UA**Ca**Gc**Ua**Au**U*●c●aL10
IX	siTTR-ESC+	antisense	VP-u●*U*●a*Ua**Ga**Gc*a*Aga**Ac**Ac**Ug**Uu*●u●u
		sense	a●a●*Ca**Gu**Gu**UC**Uu**Gc**Uc**Ua**U*●a●a
X	siTTR-LNA	antisense	VP-u●*U*●a*Ua**Ga**Gc*a*Aga**Ac**Ac**Ug**Uu*●u●u
		sense	A^{L}●A^{L}●*Ca**Gu**Gu**UC**Uu**Gc**Uc**Ua**U*●a●a
XI	siTTR-Chol	antisense	VP-u●*U*●a*Ua**Ga**Gc*a*Aga**Ac**Ac**Ug**Uu*●u●u
		sense	a●a●*Ca**Gu**Gu**UC**Uu**Gc**Uc**Ua**U*●a●aL10
XII	siGFP	antisense	P-UCCUUGAAGAAGAUGGUGCGC
		sense	GCACCAUCUUCUUCAAGGAdTdT

Notations and nomenclature: *P* = 5′-phosphate; VP = *E*-vinyl phosphonate; ● = Phosphorothioate linkage; Nucleotide, upper case letter = U,C,A,G are unmodified ribonucleotides; lower case letter = a,c,g,u are 2′-OMe modified nucleotides; italics upper case letter = *U,C,A,G* are 2′-F modified nucleotides; L10 = Cholesterol moiety; Upper case letter with superscript L = A^{L}, m5C^{L}, T^{L} are Locked Nucleic Acid (LNA)-modified nucleotides. Negative control: siTTR.

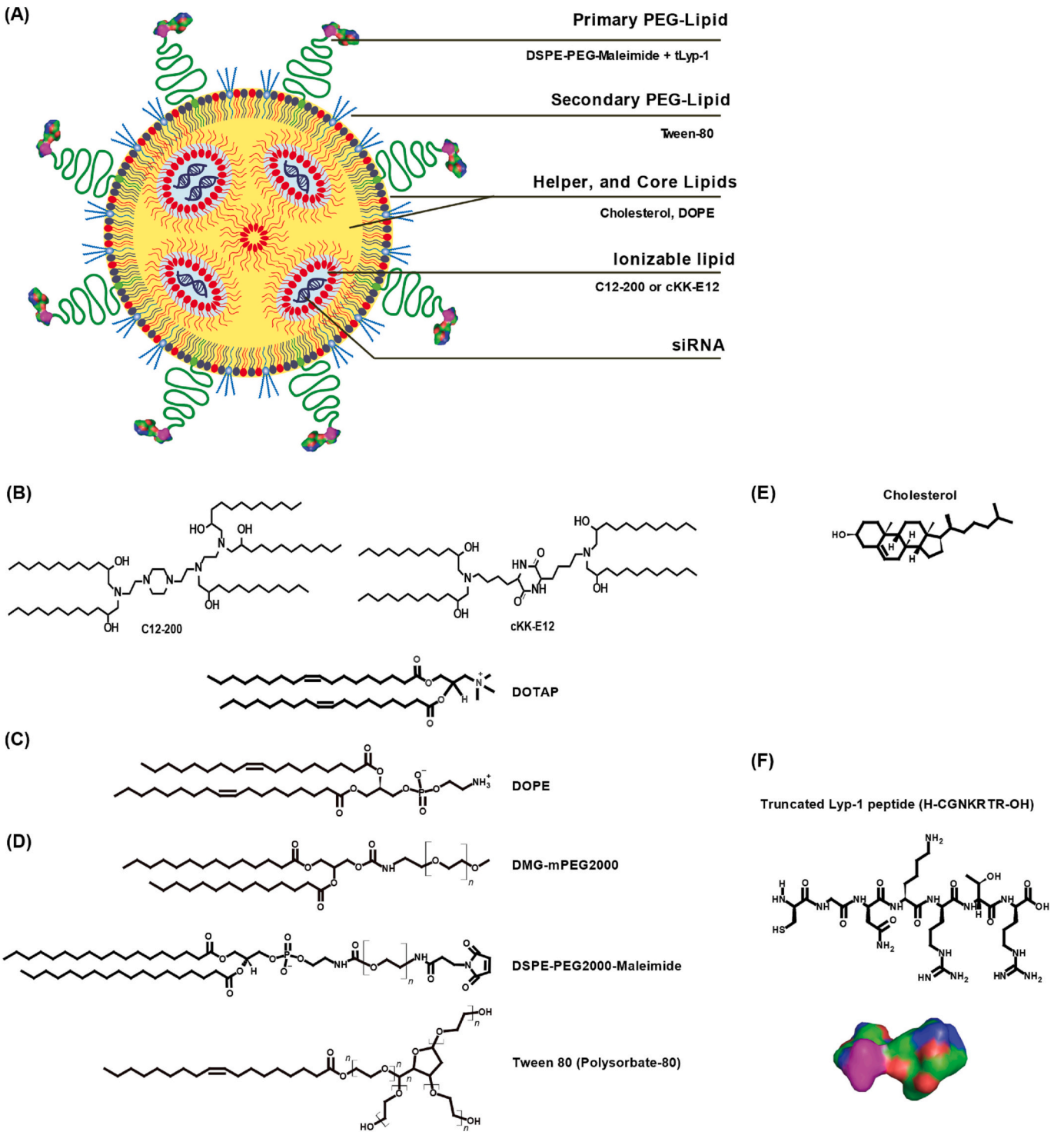

Fig. 1. Schematic representation of targeted siRNA-LNP (A) and the structure of condensing lipids (B), phospholipid (C), PEG lipids and surfactants (D), core lipids (E), and tLyp-1 targeting ligand (F) used in this study. The structure of tLyp-1 peptide was predicted using PEPstrMOD online tool [41], and the 3D-surface of the peptide was generated by the PyMOL Molecular Graphics System, Version 1.4.7.5 Edu, Schrödinger, LLC.

mg/mL) was added to an equal volume of cLNPs at a required DOTAP concentration (0.88 mg/mL) under magnetic stirring (700 RPM, 20 s). The formulations were characterized for size, zeta-potential and transfection efficiency.

2.2.2. *Preparation of siRNA loaded LNPs*

LNPs were formulated by mixing an aqueous phase containing an siRNA in citrate buffer, pH 4 (Alfa Aesar, Germany), and an organic phase containing an ionizable lipid (C12–200. HCl or cKK-E12), a phospholipid (DOPE or DSPC), cholesterol and a PEG-lipid (DMG-PEG2000, DSPE-PEG-Maleimide and/or Tween® 80) dissolved in absolute ethanol at required molar ratios [27]. In the case of preparation of cKK-E12-based LNPs, 2.5 M equivalent of hydrochloric acid was added to the organic phase to pre-protonate the amine groups of cKK-E12. The compositions of all the LNPs reported in this study are presented in Tables 2 and 3. For the toxicity study, the LNPs were either prepared at a

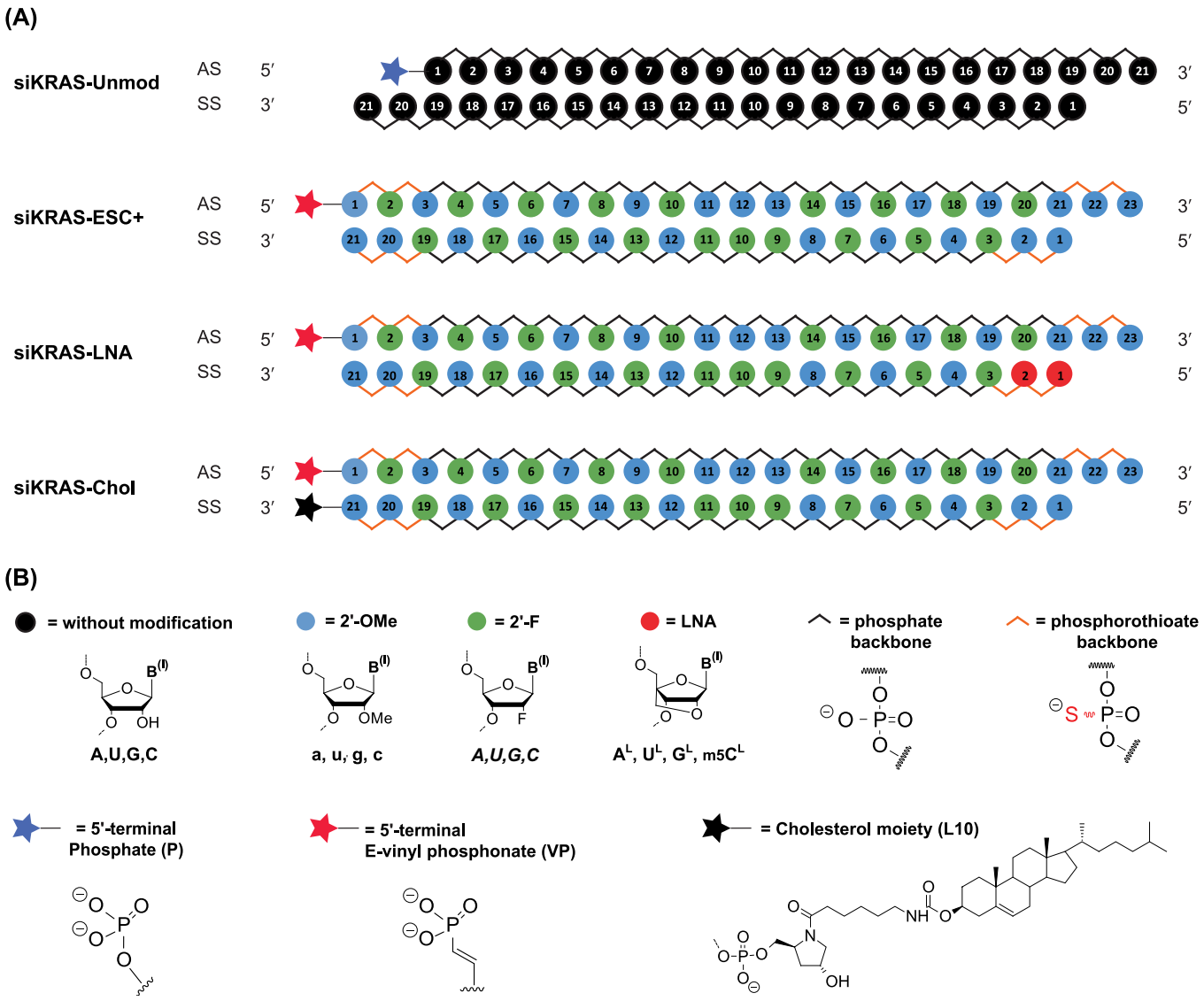

Fig. 2. Schematic representation of siRNA designs (A) and the structure of the chemical modifications (B) used in this study are presented. AS: Antisense strand; SS: Sense strand.

lower (6:1, *w*/w) or higher (12:1) mass ratio between C12–200 and RNA and were referred as LNP-Low and LNP-High, respectively. The N/P or charge ratio for LNP-Low was calculated to be around 6.76: 1, while for LNP-high was calculated to be around 13.52: 1. For the efficacy study, the LNPs were prepared at 12:1 mass ratio between C12–200 and RNA. The LNPs were formulated using a microfluidics system (NanoAssemblr BenchTop, Precision Nanosystems, Vancouver, Canada) at a final siRNA concentration of 0.1–0.4 mg/mL with a total flowrate of 9 mL/min, and a flow rate ratio of 3:1, between the aqueous and organic phase. The formulation was diluted with equal volume of 2× PBS upon preparation. For *in vivo* assays, the formulations were dialyzed (Thermo Scientific™ SnakeSkin™ 7000 molecular weight cut-off, MWCO, dialysis tubing) against PBS (1×) for two cycles (2–4 h per cycle) to remove ethanol and in some cases unbound tLyp-1 peptides. Finally, the formulation was concentrated using an Amicon® centrifugal ultrafiltration system (100 kDa nominal MWCO). The final siRNA concentration and RNA encapsulation efficiency were estimated from Ribogreen assay (Invitrogen™ Quant-it™ RiboGreen RNA Assay Kit) and agarose gel assay.

To produce fluorescent LNPs, the same protocol was used as described above, except that a fluorescent dye (DiD or DiR) was additionally included at 0.2 mol% in the organic phase along with other lipids [42]. DiD and DiR are C18-modified, lipophilic dyes that would non-covalently incorporate in the hydrophobic compartments of the LNPs. DiD with an excitation/ emission in the visible range (644/665 nm) is widely used for *in vitro* applications, while DiR a near-infrared dye (748/780 nm) is ideal for *in vivo* application where the higher wavelength light with deeper penetration properties enable easy detection of the signal in biological tissues.

The formulations were also characterized for size, and zeta-potential (Zetasizer Nano-ZS, Malvern Instruments, UK). Usually, the formulations were diluted with 1× PBS to an appropriate concentration to produce an attenuator value between 6 and 8 for size measurement, and the same dilution was used for zeta-potential measurement. For zeta-potential measurements in PBS, monomodal setting was opted as it is recommended for the samples in high ionic strength solutions (≥ 150 mM).

2.2.3. Conjugation of tLyp-1 to DSPE-PEG-Maleimide

2.2.3.1. In-situ conjugation technique. In this technique, LNPs were formulated with DSPE-PEG-Maleimide (1.5 mol%) in the organic phase as previously described. In a second step, the pH of the LNP dispersion was adjusted with HEPES buffer to pH 7–7.4, followed by the incubation

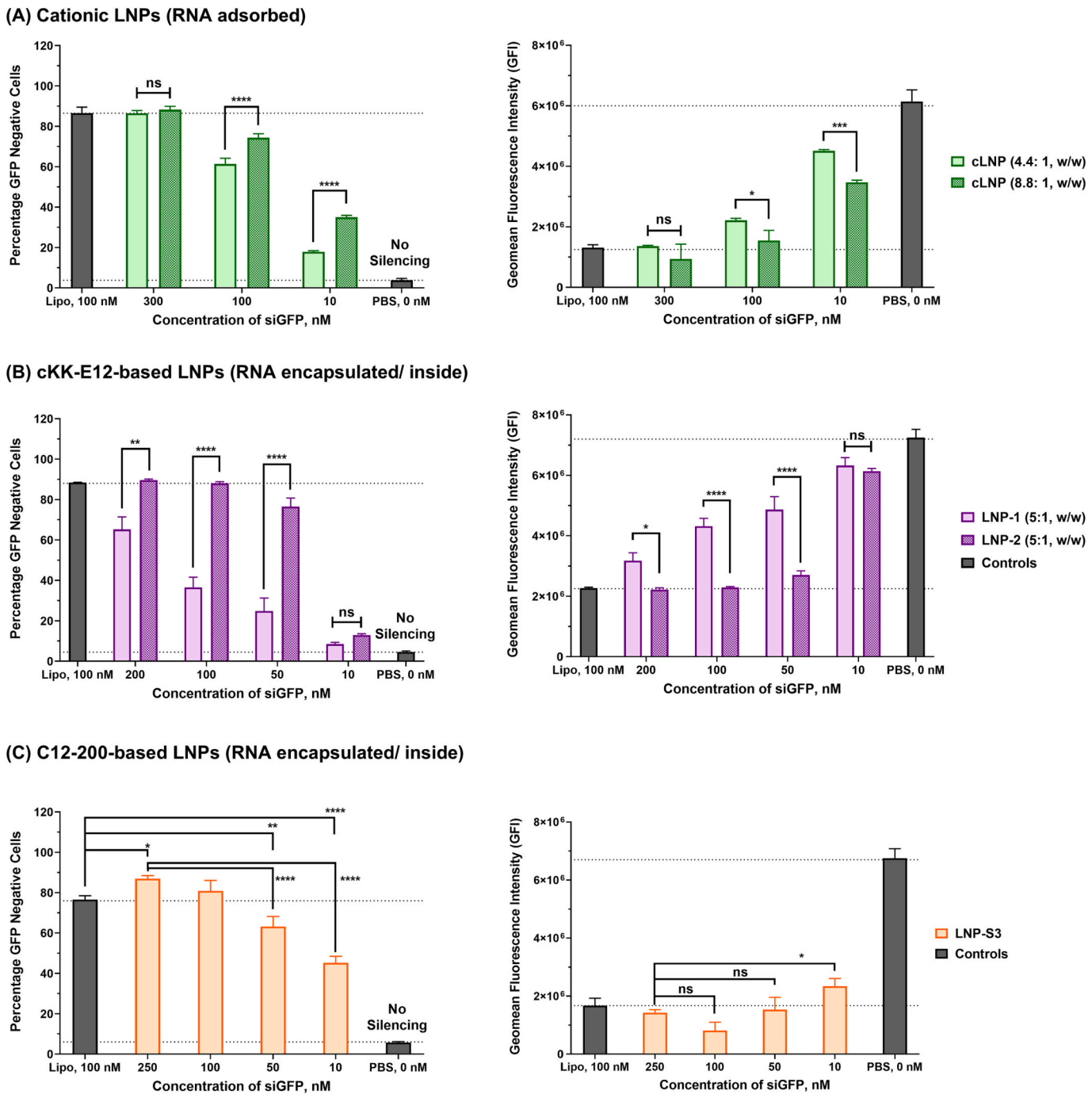

Fig. 3. Screening of formulations using *in vitro* GFP silencing assay. Percentage GFP negative cells and Geomean fluorescence intensity of DOTAP-based LNPs (A), cKK-E12 based LNPs (B), C12–200-based LNP-S3 (C) are presented. The outcome of statistical analysis (ANOVA – multiple comparison) for LNP-S3 is presented in the supplementary sections, S3-C, and S3-D. All formulations were prepared with GFP-siRNA ($N = 1$). Positive control includes treatment with Lipofectamine® RNAiMAX/siGFP at 100 nM, while the negative control includes untreated cells. Statistical significance with a $p \leq 0.05$ is represented as *; ** is $p \leq 0.01$; *** is $p \leq 0.001$; **** is $p \leq 0.0001$, $p \geq 0.05$, ns – not significant.

with 2 M equivalents of the tLyp-1 peptide for 24–48 h at +4 to +8 °C. At the end of the incubation, the LNPs (1 to 10 mL at 0.2 mg/mL) were dialyzed against PBS (200 mL) for at least 2 cycles with each cycle lasting for about 2–4 h, using a 7000 MWCO dialysis membrane. This dialysis step would effectively remove any excess tLyp-1 peptide (834 Da) from the LNPs. Finally, the dialyzed formulation was concentrated to a theoretical concentration of 0.5 to 1.5 mg/mL siRNA using an Amicon® centrifugal ultrafiltration unit (100 kDa nominal MWCO) following the manufacturers recommended protocol. The actual RNA concentration was determined using Quant-it™ RiboGreen RNA Assay Kit and diluted to the required concentration.

2.2.3.2. Pre-conjugation technique. In this technique, a DSPE-PEG-Maleimide-tLyp-1 conjugate (DPM-tLyp-1) was prepared and the conjugation of the peptide to the lipid was confirmed by NMR. This DPM-tLyp-1 conjugate was included in the organic phase during the preparation of LNPs as previously described. To prepare the DPM-tLyp-1 conjugate, a freshly prepared solution of DPM (25 mg in 60% ethanol at 1 mg/mL) was mixed with a freshly prepared solution containing a 2-M equivalent of tLyp-1 peptide with an N-terminal cysteine (14.6 mg,

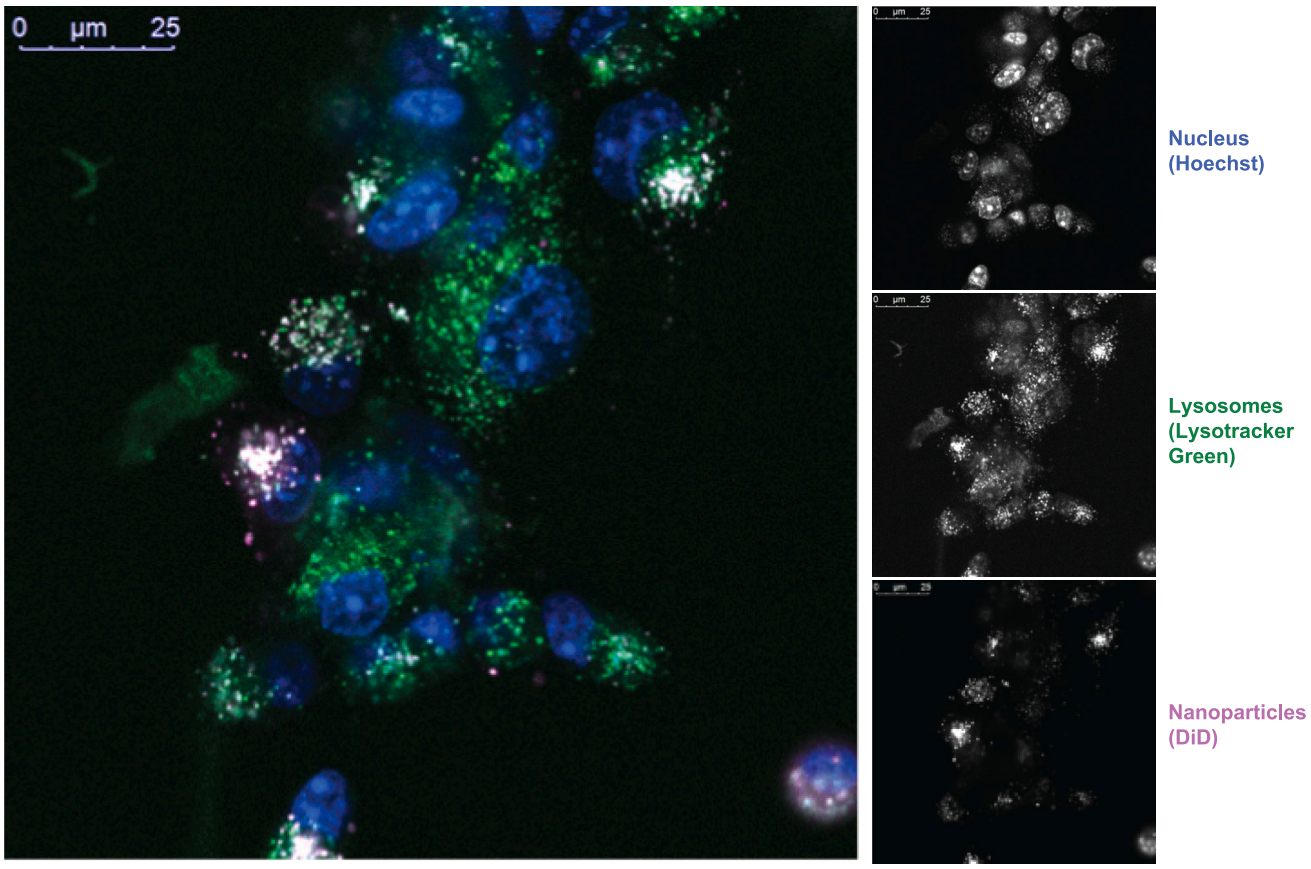

Fig. 4. *In vitro* uptake of DiD-labelled LNP-S3 4-h post-treatment. Color coding: Nucleus (Hoechst) is presented in blue, lysosomes (lysotracker green) in green and LNPs (DiD) in magenta. The white color represents the colocalization of nanoparticles and lysosomes in the endosomal vesicles. Cell line used: Lacun3 mouse lung cancer cells. The composition of LNP used in this study, LNP-S3.DiD: C12–200: DOPE: Chol: Tween® 80: DiD at 28: 14: 49.8: 8: 0.2 mol%, while the C12–200: RNA was 12:1, *w*/w. LNP-S3.DiD were treated at a concentration of 100 nM of siRNA per well. (For interpretation of the references to color in this figure legend, the reader is referred to the web version of this article.)

considering 97% purity). The mixture was incubated at room temperature for an hour under stirring, followed by incubation for about 24–48 h at +4 to +8 °C, purified with at least 3 cycles of dialysis using a 7000 MWCO dialysis membrane (1 cycle with 0.9% NaCl, 2 or more cycles with DNase/RNase/Endotoxin free Milli-Q water), and lyophilized. For proton NMR analysis, the final product was dissolved in deuterated DMSO to a final concentration of around 2 mg/mL and the conjugation efficiency was calculated with quantitative proton NMR spectrum (BRUKER DRX 500, CACTUS, USC).

2.3. *In vitro evaluation*

2.3.1. *Viability studies after anti-KRAS siRNA treatment*

A549 cells were either treated with 10 nM siRNA (siKRAS #1, siKRAS #2 or siNT) with Polyplus Transfection® agent (INTERFERin®) or with LNPs encapsulating siRNA (siKRAS #1, siKRAS #2, siNT or pI:C) at a concentration equivalent to RNA concentrations of 0.08 nM to 157.2 nM (prepared as 1:3 dilution series). Cell viability was determined with a CellTiter Glo assay kit (G9243) after 24-, 48-, 72- and 120-h post-treatment, and calculated relative to control cells, *i.e.*, as percentage of the luminescence signal of control cells.

2.3.2. *Western Blot and Colony forming assay*

Human A549 cells and murine CMT167 cells were transfected with siRNA against KRAS with INTERFERin®. KRAS knockdown efficiency and effect on proliferation (colony formation) were determined using two different custom-made siRNAs against murine KRAS (siKRAS #1, #2) or a siRNA against human and murine KRAS (siKRAS Unmod/siKRAS USC). In addition, Allstar non-target control siRNA ("siNT"), and Allstar cell death-inducing siRNA ("Cell death"/ short: death), specific for human and murine targets, respectively were used as controls.

2.3.3. *In vitro uptake study*

Lacun3 mouse lung cancer cells were seeded in a 96-well plate (5000 cells/ well). After 12–24 h of incubation, the cells were treated with DiD-labelled LNP-S3 siRNA formulation for 4 h in Opti-MEM at siRNA concentrations of 100 nM/well. After the treatment, the nanoparticle containing medium was discarded, washed twice with PBS. The cells were incubated with Hoechst (10 µg/mL) to stain its nucleus, while the acidic compartments such as lysosomes were stained with Lysotracker Green (50 nM) for 120 min. The cells were imaged using confocal imaging microscope (Leica SP8, 63 × 1.2 NA objective). The image processing was done in FIJI [43].

2.3.4. *GFP silencing study*

A total of 10,000 HeLa-GFP cells were seeded per well in a flat-bottom 96-well plate and allowed to adhere for 12–24 h. Cells were treated with siRNA formulations for 4 h in Opti-MEM at siRNA concentrations ranging from 0 to 400 nM/well. Formulations were then removed, replaced with complete medium and the cells were incubated for another 48 h. The cell viability was measured by the resazurin assay [44]. Briefly, cells were incubated with resazurin (44 µM, final concentration) supplemented complete media for 40 min, the fluorescence was measure in a plate reader at 544/590 nm. Cells were then trypsinized, harvested and fixed with 1% (*w*/*v*) formaldehyde in PBS for flow cytometry analysis. In some experiments, a total of 60,000 HeLa-GFP

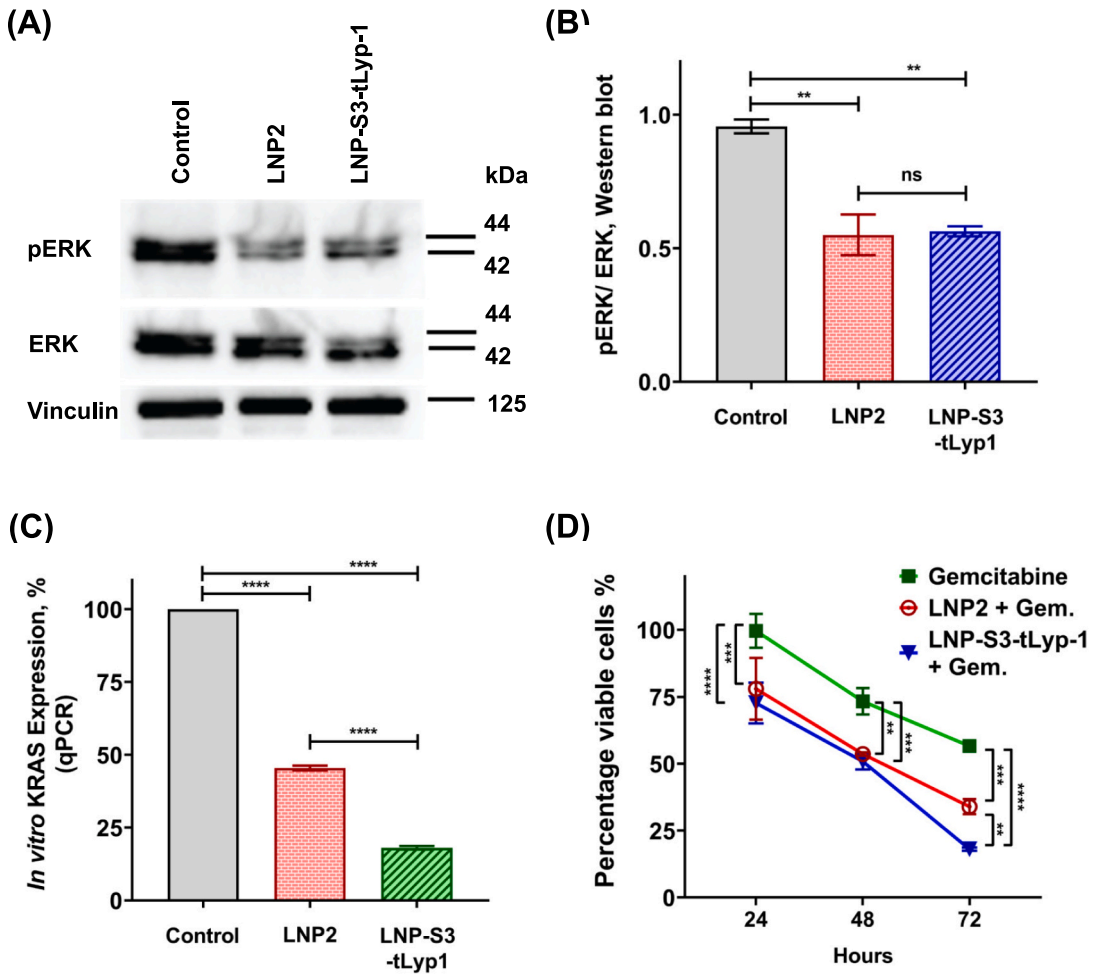

Fig. 5. *In vitro* validation of siKRAS-LNA formulated in targeted and non-targeted LNPs in CFPAC-1 pancreatic cancer cell line. Western blot comparing the total ERK, phosphoERK, and vinculin (A), Band intensity measured by Image J (B), KRAS expression measured by quantitative PCR (C), and MTT assay measuring the viability of CFPAC-1 treated with LNPs in combination with gemcitabine. Statistical significance with a $p \leq 0.05$ is represented as *; ** is $p \leq 0.01$; *** is $p \leq 0.001$; **** is $p \leq 0.0001$.

cells were seeded per well in 24-well plates. Lipofectamine RNAiMAX® at 100 nM siRNA concentration was used as a positive control following manufacturer instructions. The Hela-GFP cell line was a kind gift from Prof. Javier Montenegro, University of Santiago de Compostela.

2.3.5. Cell culture and siRNA treatment

CFPAC-1 cells were cultured in RPMI-1640 (Biological Industries, Kibbutz Beit Haemek, Israel) containing 10% FBS, 1% Pen-Strep, and 1% L-glutamine (Biological Industries) at 37 °C in a humidified 5% CO2 incubator. Cells were seeded in a 6-well plate at 5×10^5 cell/mL for western blot and qPCR analyses, and in 96-well plate at 2×10^4 cells/well for MTT assay. These cells were treated with LNP2 or LNP-S3-tLyp-1 (2000 ng/well = 137 nM). The incubation period was 24 h for western blot and qPCR analyses and 24, 48, and 72 h for MTT assay. siKRAS-LNA was used in this study.

2.3.6. Western blot analysis

Total cell lysates of siRNA-treated CFPAC-1 cells were isolated by using a lysis buffer including RIPA buffer (Thermo Fisher Scientific, Waltham, MA, USA), protease inhibitor, and phosphatase inhibitors (Roche, Basel, Switzerland). After total cell lysates were run on SDS-PAGE, they were transferred to PVDF membranes. Primary antibodies (anti-human-total ERK (1:2000), anti-human-phospho ERK (pERK-Thr202/Tyr204, 1:2000) (Cell Signaling Technology, Danvers, MA, USA), anti-human vinculin (1 μg/mL, Thermo Fisher Scientific) were used with HRP-conjugated secondary antibodies (Cell Signaling Technology). The Chemiluminescent system Newton 7.0 (Vilber, Collégien, France) was used for visualization and analyses were performed by using ImageJ software (NIH Image, Bethesda, MD, USA).

2.3.7. Real-time reverse transcription-polymerase chain reaction (qPCR)

Total RNA was isolated from siRNA-treated CFPAC-1 cells or tumors (MN, Germany) and complementary DNA was synthesized (NEB, USA). Real-time reverse transcription-PCRs were performed with SsoAdvanced™ Universal SYBR Green Super Mix (Bio-Rad, USA) and carried out on a CFX Connect Real Time PCR (Biorad, USA). The gene expression of KRAS (forward 5'-GACTCTGAAGATGTACCTATGGTCCTA-3′, reverse 5'-CATCATCAACACCCTGTCTTGTC-3′) was determined compared to beta-actin (forward 5'-CTGGAACGGTGAAGGTGACA-3′ reverse 5'-AAGGGACTTCCTGTAACAATGCA-3′). The relative difference in gene expression was calculated with comparative $2^{(-\Delta\Delta Ct)}$ method where amplification data obtained from the gene of interest were normalized to beta actin housekeeping gene expression (ΔCt = Ct (KRAS) – Ct (beta-actin)) and then with the data from control (untreated) samples (ΔΔCt = ΔCt (siKRAS treated sample) – ΔCt (untreated sample)). Control sample data was set to have 100% expression and other groups were normalized to control group for illustration.

2.3.8. Methylthiazolyldiphenyl-tetrazolium bromide (MTT) assay

The MTT assay was used to assess cytotoxicity. MTT solution

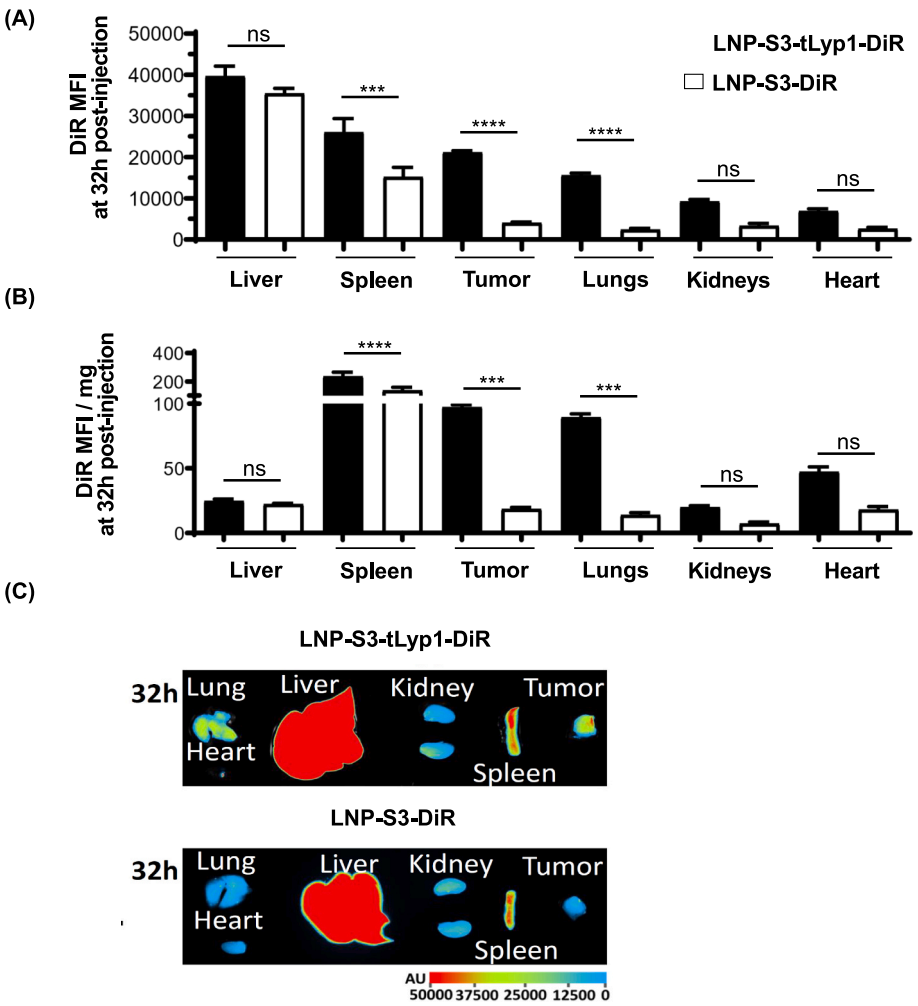

Fig. 6. *In vivo* biodistribution of siRNA loaded LNPs labelled with a fluorescent dye (DiR). The mean fluorescence intensity (MFI) from DiR measured from different organs (A); The MFI normalized to the mass of each organ (B); and IVIS image of the organs (C). *** $p < 0.001$, **** $p < 0.0001$, ns – not significant. (Number of mice per group, $n = 4$, Dose: 100 μL of LNPs at 1 mg/mL siRNA concentration). Targeted LNP: LNP-S3-tLyp1-DiR, non-targeted LNP: LNP-S3-DiR.

(Sigma–Aldrich, St. Louis, MO, USA) was added into the wells and incubated for 4 h. Lysis buffer containing 23% SDS and 45% *N,N*-dimethylformamide (Sigma-Aldrich) was added to dissolve formazan crystals and incubated for 16 h. Optical densities (OD) were acquired at 570 nm by a Spectramax Plus microplate reader (Molecular Devices, Sunnyvale, CA, USA). The percentages of the number of viable cells were calculated according to the cells incubated with culture medium only.

2.3.9. Immunofluorescence staining

Frozen sections of the tumors (Leica Microsystems, Nussloch, Germany) were fixed with 4% paraformaldehyde and blocked with 10% BSA. They were incubated with anti-human-pERK (Cell Signaling Technology) primary antibody and antibody binding was visualized by Alexa555-conjugated secondary antibody (Abcam, Cambridge, United Kingdom) together with DAPI (Sigma–Aldrich). Images were taken with a fluorescence microscope (Olympus, Center Valley, PA, USA) and analyses were performed by using ImageJ software (NIH Image).

2.3.10. Flow cytometry

The cells were labelled with mouse anti-human-Neuropilin-1 (Nrp-1)-PE (clone:12C2) (BioLegend, San Diego, CA, USA). Percentages of positive cells were determined according to an isotype control antibody. The analyses were performed with a FACS Canto II (Becton Dickinson, San Jose, CA, USA).

2.4. Animal studies

All animal procedures were performed in compliance with relevant laws and institutional guidelines and the appropriate institutional committee(s) have approved them.

2.4.1. In vivo biodistribution - Pancreatic cancer model

A xenograft tumor model was developed using 6–8 weeks old athymic CD1 nude mice to study biodistribution and the antitumoral efficacy of the combination treatment: gemcitabine and anti-KRAS siRNA. After subcutaneous injection of 1.5×10^7 pancreatic CFPAC1 cells in 100 μL PBS with 1 mg/mL Matrigel to the dorsal flank of mice, tumor development was followed until reaching 0.7 cm diameter. Mice were intravenously injected with a single dose of fluorescently labelled LNPs at dose of 3.33 mg/kg (100 μL of LNPs at 1 mg/mL siRNA concentration). The mice were euthanized, and organs were collected 32 h post injection and the fluorescence in individual organs was measured using an *in vivo* imaging system (IVIS). The composition of LNPs used in this study are presented in Table 3.

2.4.2. In vivo efficacy studies - Pancreatic cancer model

2.4.2.1.

A xenograft tumor model was developed as previously described for the biodistribution study (Kobay experimental animals ethical council

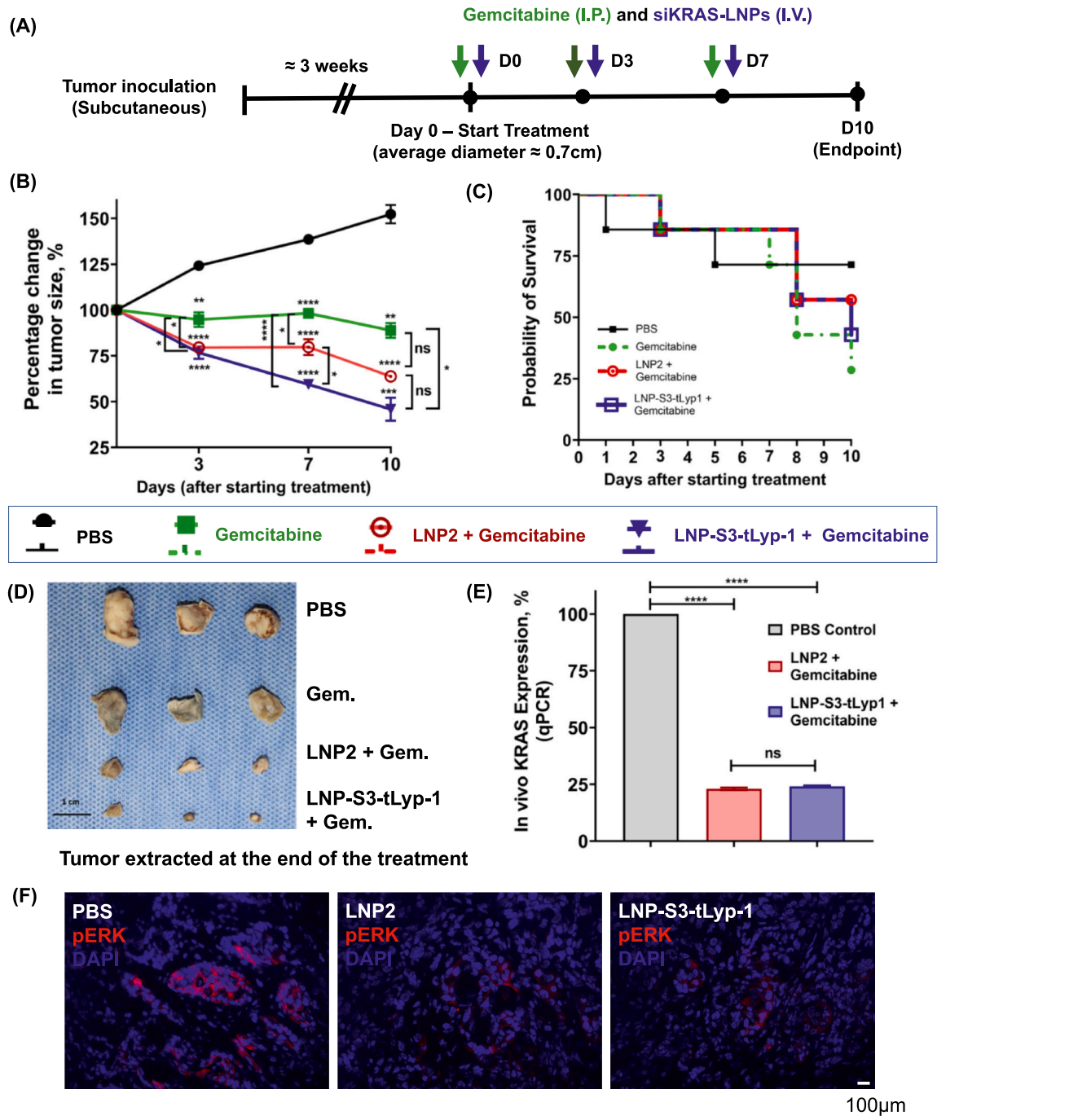

Fig. 7. Therapeutic effect of the combination treatment with gemcitabine and siKRAS. Experimental set-up indicating tumor inoculation, days of treatment and endpoint of the study (A); percentage change in tumor volume. The stars indicating the statistical differences between the PBS control verses other groups are presented just above each symbol, while other comparisons are indicated with a line and star(s) (B), Survival plot (C); image of the tumors extracted at the end of the experiment (D); KRAS expression measured by qPCR, $n = 3$. Statistical test: unpaired two-tailed *t*-test (E), and immunofluorescence of pERK in tumors, where pERK labelling is presented in Red, while the nucleus stained with DAPI is presented in Blue (F). Dosing: Gemcitabine (100 μL per injection at 25 mg/mL gemcitabine in saline, ≈ 100 mg/kg) was administered intraperitonially, while targeted and non-targeted LNPs encapsulating siKRAS-LNA (50 μL per injection at 0.8 mg/mL in PBS ≈ 1.3 mg/kg) were administered intravenously on Day 0, Day 3, and Day 7 (Number of mice per group, $n = 7$). Statistical significance with a $p \leq 0.05$ is represented as *; ** is $p \leq 0.01$; *** is $p \leq 0.001$; **** is $p \leq 0.0001$, $p \geq 0.05$, ns – not significant. (For interpretation of the references to color in this figure legend, the reader is referred to the web version of this article.)

project number 2017/232). Mice were separated into groups randomly (7 mice per group). Gemcitabine was injected intraperitoneally (i.p.), while controls, and LNPs loaded with anti-KRAS siRNA were injected intravenously (i.v.) twice a week. Gemcitabine was administered at a dose of 100 mg/kg, while mice were treated with 50 μL of LNPs at 0.8 mg/mL siRNA concentration (1.33 mg/kg). Two different administration routes were chosen to avoid any interaction between the drug and the LNP which may affect their pharmacokinetics. Additionally, LNPs are generally administered I.V. for many applications [22], while intraperitoneal administration of gemcitabine is an emerging and effective alternative route of administration for pancreatic cancer [45]. Tumor volume, animal weight and health conditions were monitored

Table 2
Physicochemical characteristics of siRNA formulations tested by *in vitro* GFP or KRAS silencing assay. ($N = 1$).

Code	Components	Molar % (CL: RNA, *w/w*)	Prep. Technique	[RNA] mg/mL	Size (nm)	PDI	ZP.PBS (mV)	siRNA	[N/P ratio]
Cationic DOTAP LNPs									
cLNP (2:1)	DOTAP: DOPE: Cholesterol: Tween® 80	27.1: 12.7: 52: 8.1 (4.4:1, w/w)	Stirring	0.1	153 ± 3	0.17 ± 0.01	+33 ± 3	siGFP	2:1
cLNP (4:1)	DOTAP: DOPE: Cholesterol: Tween® 80	27.1: 12.7: 52: 8.1 (8.8:1, w/w)	Stirring	0.1	121 ± 3	0.21 ± 0.02	+34 ± 1		4:1
cKK-E12 LNPs									
LNP-A	cKK-E12: DSPC: Cholesterol: DMG-PEG	50: 10: 38.5: 1.5 (5:1, w/w)	Microfluidics	0.05	84 ± 1	0.16 ± 0.01	−0.6 ± 0.9	siGFP	3.2: 1
LNP-B	cKK-E12: DOPE: Cholesterol: DMG-PEG	35: 16: 46.5: 2.5 (5:1, w/w)	Microfluidics	0.05	56 ± 1	0.08 ± 0.01	−0.5 ± 0.6		3.2: 1
C12–200 LNPs									
LNP-S3	C12–200: DOPE: Cholesterol: Tween® 80	28: 14: 50: 8 (12:1, w/w)	Microfluidics	0.1	59 ± 1	0.09 ± 0.003	−1.6 ± 0.6	siGFP	13.1: 1
				0.1	53 ± 1	0.15 ± 0.02	−2.7 ± 0.8	siKRAS-ESC+	13.6: 1
				0.1	56 ± 2	0.13 ± 0.03	−0.8 ± 0.7	siKRAS-LNA	13.6: 1
				0.1	56 ± 1	0.22 ± 0.01	−1.7 ± 0.4	siKRAS-Chol	14.2: 1
C12–200 LNPs used for the *in vitro* uptake study									
LNP-S3. DiD	C12–200: DOPE: Chol: Tween® 80: DiD	28: 14: 49.8: 8: 0.2 (12:1, w/w)	Microfluidics	1.8	59 ± 1	0.12 ± 0.02	−1.5 ± 0.1	siKRAS-LNA	13.6: 1

Abbreviations: CL: ionizable cationic lipids. cLNPs: cationic LNP with adsorbed RNA. n.d.: not determined/or no data. Stirring: Magnetic stirring (700 RPM, 10 s); Microfluidics: NanoAssemblr BenchTop.

after each injection.

2.4.3. *In vivo* toxicity evaluation

The *in vivo* study was carried-out in healthy immunocompetent female ICR Swiss mice (7–8 weeks old). All animal procedures were approved by University of Santiago de Compostela Bioethics Committee in compliance with Principles of Laboratory Animal Care of national laws. Mice were split into one untreated control group and two treatment groups ($n = 4$ mice per group). One treatment group received LNP2-Low (C12–200: RNA at 6:1, *w*/w), while the other group received LNP2-High (C12–200: RNA at 12:1, w/w), both formulated using the same optimized molar lipid composition reported in the literature [27], the detailed compositions and characteristics are presented in Table 3. This optimized molar composition allowed maximum siRNA encapsulation at both the high and low mass ratios tested here, Table 3 and **supplementary data - Fig. S9**. LNPs were administered intravenously twice a week, for 4 weeks (8 doses). Both the treatment groups received the same dose of siRNA (100 μL per injection at 0.4 mg/mL siRNA encapsulated in LNPs corresponding to a dose of about 1.33 mg/kg of siRNA for a 30 g mouse) while receiving different doses of ionizable lipid (2.4 or 4.8 mg/mL of C12–200, corresponding to a dose of about 8 or 16 mg/kg of C12–200 for LNP-Low and LNP-High groups respectively). This experimental approach was expected to allow unbiased toxicity from the lipids, as the siRNA dose in both treatment groups is constant. Animals were monitored daily for clinical signs and weighed twice a week (before injection). Mice were sacrificed 4 days after the last treatment; organs (liver, spleen, and kidneys) and blood samples were collected for histochemistry (hematoxylin and eosin staining), hematology (BC-5000Vet-Mindray) and biochemistry analysis (Preventive Care Profile Plus, Vetscan, Abaxis).

2.5. Statistical analysis

The statistical tests were performed with GraphPad Prism 8.0.2. For *in vitro* GFP-silencing assay, the results were analyzed by ordinary Two-Way ANOVA. Statistical significance between the groups corresponding to the same dose treatment were determined using the Sidak multiple comparison method. The multiplicity adjusted *P* value are reported, where alpha (significant difference) was set to 0.05. For *in vitro* and *in vivo* KRAS expression by qPCR, *in vitro* pERK expression in the *in vivo* efficacy study, comparison of between the groups were made with ordinary Two-Way ANOVA using Turkey's multiple comparison. Of note, both Turkey's and Sidak multiple comparisons produced same significant differences. For *in vivo* toxicity study, the exact *p* values were determined using unpaired multiple *t*-test where each row (biochemical or hematological parameter) was analyzed individually without assuming a consistent standard deviation (SD). Statistical significance between the groups was determined using the Holm-Sidak method to calculate the multiplicity adjusted P value. For *in vivo* efficacy study, the evolution of tumor volume was analyzed using a mixed-effect model with Tukey's multiple comparisons test.

Throughout the manuscript, alpha (significant difference) was set to 0.05, and the statistical differences are represented as follows, * $p < 0.05$, ** $p < 0.01$, *** $p < 0.001$, **** $p < 0.0001$, ns – not significant.

3. Results and discussion

The aim of this work is to identify a suitable anti-KRAS siRNA, engineer the LNPs to improve siRNA delivery to tumors, evaluation of *in vivo* toxicity of C12–200 based siRNA-LNPs and evaluate the therapeutic benefits of KRAS silencing in KRAS-mutant cancer models. To do this, we followed a specific work plan consisting of: (i) the development of different LNP formulations and the evaluation of their physicochemical properties, stability and transfection capacities using model RNA molecules, (ii) the functionalization of selected LNP compositions with the targeting peptide tLyp-1, (iii) The chemical modification and evaluation of different anti-KRAS siRNA molecules and their encapsulation into selected LNP prototypes, (iv) the *in vivo* evaluation a selected prototype containing a selected siRNA anti-KRAS sequence for its biodistribution and efficacy in a pancreatic tumor mice model.

Table 3
Physicochemical characteristics of siRNA formulations tested in various *in vitro* and *in vivo* assays.

Code	Components	Molar % (CL: RNA, *w/w*) [N/P ratio]	Prep. Technique	[RNA] mg/mL	Size (nm)	PDI	ZP.PBS (mV)	% Encap. RNA (Ribogreen)	N	siRNA cargo
LNPs used for the *in vivo* biodistribution study										
LNP-S3-DiR	C12–200: DOPE: Chol: Tween® 80: DiR	28: 14: 49.8: 8: 0.2 (12:1, w/w) [13.57: 1, N/P]	Microfluidics	1	68 ± 2	0.12 ± 0.01	−0.7 ± 0.6	95	1	siKRAS-ESC+
LNP-S3-tLyp-1-DiR	(C12–200: DOPE: Chol: Tween® 80: DiR: DPM) + tLyp-1, *in-situ* conjugation	28: 14: 49.8: 6.5: 0.2: 1.5 (12:1, w/w) [13.57: 1, N/P]		1	51 ± 1	0.14 ± 0.01	+3 ± 0.1	95	1	
LNPs used for *in vitro and in vivo* efficacy study (CFPAC-1, pancreatic cancer model)										
LNP2	C12–200: DOPE: Chol: DMG-PEG	35: 16: 46.5: 2.5 (12:1, w/w) [13.59: 1, N/P]	Microfluidics	0.8	64 ± 2	0.15 ± 0.03	−0.3 ± 1	89 ± 1	2	siKRAS-LNA
LNP-S3-tLyp-1	C12–200: DOPE: Chol: Tween® 80: DPM + (tLyp-1) – *in-situ* conjugation	28: 14: 50: 6.5: 1.5 (12:1, w/w) [13.59: 1, N/P]		0.8	60 ± 3	0.16 ± 0.02	+3 ± 1	93 ± 2	2	
LNPs used for the *in vivo* toxicity study										
LNP2-Low	C12–200: DOPE: Chol: DMG-PEG	35: 16: 46.5: 2.5 (6:1, w/w) [6.76: 1, N/P]	Microfluidics	0.4	64 ± 6	0.15 ± 0.02	−0.5 ± 0.5	79 ± 1	2	siTTR-ESC+
LNP2-High		35: 16: 46.5: 2.5 (12:1, w/w) [13.52: 1]			59 ± 5	0.10 ± 0.03	−0.3 ± 0.9	91 ± 1	2	

Abbreviations: CL: permanently- or ionizable cationic lipids. cLNPs: cationic LNP with adsorbed RNA. Microfluidics: NanoAssemblr BenchTop. N/P ratio: Ratio between cationic/ ionizable nitrogen groups from cationic lipids to negatively charged phosphate groups from RNA.

3.1. Development and characterization of different LNP compositions containing a model siRNA

Condensing lipids are one of the key components of RNA delivery systems and in most cases a key determinant of their delivery efficacy [28,46–48]. We developed formulations for siRNA delivery based on three different condensing lipids, namely DOTAP, cKK-E12, and C12–200. The structure of the lipids used in this study are presented in Fig. 1. We also tested different PEG-lipids or surfactants such as Tween® 80, DMG-PEG2000, and DSPE-PEG-Maleimide. An *in vitro* GFP silencing assay was used for an initial screening of these formulations. We classified the array of formulations produced based on the cationic lipid used as described below.

DOTAP-based LNPs (RNA adsorbed): DOTAP is a cationic lipid with a degradable ester linkage between the hydrophobic tails and the polar head group [49]. DOTAP is a standard reference lipid whose synthesis was first reported in 1988 [50] and has been widely used as a transfection reagent [51]. Previous reports have shown that the adequate combination of cholesterol and DOTAP in lipid formulations led to an improved transfection efficiency in the presence of serum [52]. In addition, the inclusion of certain amounts of DOPE and Tween® 80 in DOTAP-containing formulations has been shown to reduce toxicity and improve *in vitro* transfection [53]. Based on these promising results and the fact that DOTAP-based formulations have been tested for several application including cancer gene therapy [54], DNA vaccines [55], and mRNA delivery [56], we chose DOTAP as a condensing lipid and added DOPE, cholesterol, and Tween® 80 in the formulation of siRNA-loaded LNP prototypes. The ratio between the cationic nitrogenous groups (N) from the ionizable/cationic lipids of the delivery system to the negative charges from the phosphate groups (P) of the RNA cargo is defined as N/P ratio (or charge ratio, +/−). In our formulation approach, the siRNA was mixed with preformed cationic LNPs (cLNPs) either at a lower or higher N/P ratios. The results presented in Table 2 indicate that higher N/P ratio (4:1, N/P or 8.8:1 *w*/w, DOTAP: RNA) showed slightly smaller size than the lower N/P ratio (2:1, N/P or 4.4:1, *w*/w).

The siRNA-loaded DOTAP-based LNPs were prepared in two steps. In the first step, a blank cationic nanosystem was prepared with DOTAP, and in the second step, the RNA was added to the system with an excess of positive charge (achieved for N/P ratio 2:1 and 4:1) which allow the adsorption of RNA to LNP surface. Agarose gel electrophoresis confirmed that there were no free RNA (data not shown), thus that the RNA molecules were associated to the LNP surface. Hence, these formulations were indicated as “RNA adsorbed”.

In other formulations containing ionizable lipids such as cKK-E12 or C12–200, the RNA molecules were incorporated inside the LNPs as previously described (27) and, hence these formulations were named as “Encapsulated RNA or RNA inside”. In this case, the procedure involved the dissolution of RNA an acidic medium (pH 4) in order to facilitate the interaction with the ionizable lipids C12–200 and cKK-E12, with a pKa ≤ 7 [27,46,57,58]. Since, no free RNA was seen in the LNP formulations after pH neutralization, it is inferred that the RNA was encapsulated inside the LNPs (RNA inside). This is in line with the literature on LNPs [27,28,46].

cKK-E12-based LNPs: (Encapsulated RNA/ RNA inside) cKK-E12 is a potent multi-tailed ionizable lipopeptide previously used for both siRNA and mRNA delivery [28,59]. Here, we compared two compositions

reported in the literature [22,27,46]. One of them, referred here as LNP-A or classical composition, is the most widely used LNP composition for two-tailed lipids, consists of ionizable-lipid, phospholipid, cholesterol, and a PEG-lipid with a molar ratio of 50:10:38.5:1.5 [22,46]. The other one, referred here as LNP-B, comes from a design of experiment (DoE) reported in the literature with a composition consisting of C12–200: DOPE:Cholesterol:PEG-lipid at a molar ratio of 35:16:46.5:2.5 [27]. These two formulations LNP-A and LNP-B were loaded with siRNA-GFP (siGFP). Both showed good physicochemical characteristics with a size below 90 nm, low polydispersity index (PDI $<$ 0.2); however, the encapsulation efficiency, using either Ribogreen or agarose gel assays, was significantly higher for the LNP-2 composition, Table 2-B, and supplementary Fig. S1.

C12–200-based LNPs: (Encapsulated RNA/ RNA inside) C12–200 is a potent multi-tailed ionizable lipidoid previously used in the literature both for siRNA and mRNA delivery [27,48]. Based on our previous experiments (unpublished data), in the present work, Tween® 80, a surfactant with a branched low molecular weight PEG (predicted log D, pH 7.4 = 5.45), was explored as an alternative PEG lipid to the classical C14-PEG (predicted log D, pH 7.4 = 6.53, ChemSpider version 2021.0.29.0). This new formulation, named as LNP-S3, was prepared with C12–200, DOPE, Cholesterol, and Tween® 80 at a molar ratio of 28:14:50:8. The results, presented in Table 2, indicate that this formulation showed good physicochemical characteristics in terms of size, zeta potential, RNA loading and stability.

The three categories of formulations described above were loaded with siRNA-GFP and tested for their *in vitro* GFP-silencing capacity. The results, shown in Fig. 3, indicate that the strongest GFP-silencing effect obtained at the lowest concentration tested (10 nM) was observed for the LNP-S3 prototype. Hence, this prototype was selected as the lead candidate for the next step, which was the functionalization of the prototype with a targeting ligand.

3.2. Development of a targeted nanocarrier based on the conjugation of a tLyp-1 to LNPs

Reaching extrahepatic targets is of great interest for developing the next generation of RNA therapeutics. With our aim to improve the intratumoral accumulation of siRNA-nanoparticles, we chose the truncated-Lyp-1 (tLyp-1) as a targeting ligand, due to its ability to interact with the neuropilin-1 (NRP-1) receptor. The presence of this receptor in the CFPAC-1 pancreatic cancer cell line, used in our *in vivo* studies, was confirmed (supplementary data – Fig. S7).

Prior to the functionalization of the LNPs with the targeting ligand, it was important to select an appropriate PEG-lipid. It is known that C14-PEG, the most frequently used PEG-lipid, is easily desorbed from LNP surface, which facilitates ApoE binding, thereby increasing liver accumulation [22,24,60]. However, as our target was not the liver, we selected a slow-desorbing C18-PEG (DSPE-PEG-Maleimide) in order to minimize the desorption of the targeting ligand from the LNP surface. For the functionalization of the LNPs with the tumor targeting ligand (tLyp-1), we used two methodologies*: (i) In situ* conjugation, a methodology that allows the direct conjugation of a thiol containing targeting ligand to a preformed nanosystem containing DSPE-PEG-Maleimide (DPM) as an anchor lipid. Here, thiol-maleimide click chemistry was used for conjugating the ligand to the anchor lipid. (ii) Pre-conjugation, a methodology that consists of the conjugation of the targeting ligand to one of the components of the LNP, in our case the DSPE-PEG-Maleimide. The efficiency of the conjugation process was determined by Proton NMR analysis. The reaction conditions were optimized to achieve a conjugation efficiency >75% as measured by NMR, supplementary data - Fig. S2.

Initial results showed that, irrespective of the conjugation method used, LNPs (C12–200, DOPE, Cholesterol, DPM at 28.2: 14.1: 56.2: 1.5 mol%) aggregated in the presence of the cationic tLyp-1. Alternatively, a pre-conjugated DPM-tLyp-1 was added directly to the organic phase to prepare an LNP with a different molar ratio; This formulation containing C12–200, DOPE, Cholesterol, DMG-PEG, and DPM-tLyp-1 at a molar ratio of 35:16:46.5:1:1.5, also aggregated upon dilution in PBS. The rationale for this was that the arginine containing cationic tLyp-1 could interact with DOPE on the LNP surface resulting in aggregation (CGNKRTR, theoretical pI = 10.86 [61]). Similar aggregations were reported when mixing arginine-rich protamine with phosphoethanolamine (PE) containing phospholipids but not with phosphocholines or sphingomyelins [62]. When the pre-formed LNPs containing Tween® 80 (LNP-S3 with DPM) were mixed with tLyp-1 peptide no aggregation was observed. Hence, the presence of Tween® 80 in the LNP composition solved this problem. This allowed the *in-situ* conjugation of the ligand to the LNPs. Similarly, when the LNPs were directly prepared with pre-conjugated DPM-tLyp-1 in the presence of Tween® 80 in the organic phase, no aggregates were formed in these formulations. DOPE has a net neutral charge around pH 7.4. This includes one positive charge from the ethanolamine, (pKa ≈ 9.5, based on ethanolamine), and one negative charge from the phosphate, (pKa ≈ 1–2.2, [63]). We hypothesize that the short PEG chains of Tween80 would allow the electrostatic interaction of tLyp-1 and DOPE while preventing the interaction among particles through stearic hinderance thus preventing aggregation. The final composition of this formulation, we called LNP-S3-tLyp-1, was C12–200, DOPE, Cholesterol, Tween® 80, and DPM-tLyp-1 at a molar ratio of 28: 14: 50: 6.5: 1.5.

Since, tLyp-1 was cationic in nature, in order to minimize its interaction with the RNA molecules during the LNP formation, we decided to conjugate the targeting ligand after the formation of LNP using the *in-situ* conjugation technique for both our *in vitro* and *in vivo* studies.

The tLyp-1 attaches to DPM *via* thiol-maleimide click chemistry yielding a thiosuccinimide covalent conjugate. Due to the very small size of the tLyp-1 peptide (7 aminoacids) and its low concentration, when compared to the rest of the LNP components, the development of an analytical technique for the quantitative verification of the ligand attachment was challenging. Both, NMR and peptide quantification by 3-(4carboxybenzoyl)quinoline-2-carboxaldehyde) (CBQCA reagent) failed to reliably quantify the amount of tLyp-1 attached to the LNPs (data not shown). Hence, as shown in Table 3, the effective attachment of cationic tLyp-1 to the neutral LNPs was indirectly inferred from a slight change in the zeta potential of the LNPs.

Taking all this into consideration, here we describe a new composition of LNPs that includes Tween® 80. The desorption rates of Tween® 80 from the LNP surface are not known and could be of interest to investigate them in the future. Inclusion of Tween® 80 in the formulation was critical to maintain the stability of tLyp-1 tagged LNPs, and we expect that this formulation can be applied to other targeting ligands.

3.3. In vitro evaluation of siRNA formulations with a model RNA

In vitro GFP silencing assays could be a valuable tool for the initial screening of the siRNA-loaded formulations. We used anti-GFP siRNA (siGFP) as a model RNA and HeLa-GFP as a model cancer cell line. Good silencing activity was seen for all the formulations (Fig. 3). For cLNPs, the higher N/P ratio (4:1, +/−) showed slightly higher silencing than the lower N/P ratio (2:1, +/−) at lower concentration (10 nM), (Fig. 3-**A**). For cKK-E12-based LNPs, LNP-B formulation was found to be superior to the LNP-A composition in terms of transfection efficiency (Fig. 3-**B**). This might be related to the higher RNA encapsulation efficiency of this formulation (**supplementary data, Fig. S1**). On the other hand, the C12–200-based formulation (LNP-S3) showed high, dose-dependent GFP silencing (Fig. 3-**C**). In fact, this formulation showed the strongest GFP-silencing, even at the lowest concentration tested (10 nM) and, therefore, was selected as the lead candidate.

To study the *in vitro* uptake of LNP-S3, the formulation was labelled with a C18-modified carbocyanine dye (DiD at 0.2 mol%) as previously described [42]. The results obtained in a murine lung cancer cell line, Lacun3, showed that the LNP-S3 uptake was high and exhibited a

perinuclear localization in the cell. At 4-h post-treatment, a strong colocalization of the LNPs with the lysosomes was observed (as a white signal by overlay of DiD and lysotracker) (Fig. 4), a result that agrees with previous findings reported in the literature [64,65]. Although in-depth trafficking studies might be required to probe the mechanism of uptake and endosomal escape, the successful *in vitro* GFP silencing (Fig. 3-**C**) indicated that siRNA-GFP was successfully released into the cytoplasm to cause gene-silencing in HeLa-GFP cells after uptake. Because of the successful uptake and silencing with siRNA-GFP loaded LNP-S3 we observed, this formulation was selected for the encapsulation of different versions of chemically modified anti-KRAS siRNAs.

3.4. Selection of siRNA candidates – In vitro evaluation and validation

An *in vitro* assay was performed to identify the most promising siRNA constructs and the appropriate chemical modifications that could efficiently silence KRAS genes and down-regulate downstream signaling (ERK1/2 (p44/p42)-phosphorylation by immunoblotting). Cells were transfected with different anti-KRAS siRNAs, using either a commercial transfection reagent (INTERFERin) or the LNPs prepared in this work. During the initial screening, western blot analysis confirmed that all KRAS-specific siRNAs were able to reduce the KRAS expression in several cell lines, including human lung cancer cell lines (A549, H441), and mouse lung cancer lines (CMT-167, Lacun3) (**supplementary data – Fig. S3**) Interestingly, the negative control siRNAs used in this study (siTTR-ESC+ and siTTR-LNA) were also able to reduce KRAS-levels in the human cancer cell line (A549) but not in the CMT-167. This behavior could be explained by the guide strand mediated microRNA-like seed-based base-paring (6–8 nucleotides) (**supplementary data - Fig. S4)**. Due to the variation in silencing between the cell lines, we decided to not to use the siTTR as the control siRNA for further studies. The down-regulation of phosphoERK provided variable results among the different treatment groups and cell lines (**supplementary data - Fig. S4).**

Despite the RNAi-mediated downregulation of KRAS, no significant effect on cell viability was observed on A549 cells treated with anti-KRAS siRNA under the tested conditions (**supplementary data - Fig. S3**, ATP measurement with CellTiter Glo assay). However, siKRAS treatment reduced proliferation in the colony forming assay (**supplementary data - Fig. S4 and S5**). A combined reduction of KRAS and phosphoERK seemed to correlate well with reduced proliferation and *vice versa*. For example, marked reduction in KRAS expression was seen in CMT-167 cells following siKRAS treatment, while phosphoERK levels were not affected (**supplementary data - Fig. S4**). These results indicate that phosphoERK might be a determining factor for *in vitro* cellular proliferation.

To identify the best siRNA candidate for *in vivo* studies, the knock-down efficacy of different versions of the anti-KRAS siRNAs were compared. The general trend in silencing efficacy we observed was consistently better for siKRAS-ESC+ (advanced enhanced stabilization chemistry plus) followed by siKRAS-LNA (locked nucleic acid modified ESC+ siRNA), unmodified siRNA (siKRAS-USC) and frequently a lower performance from the cholesterol modified-siRNA (siKRAS-Chol). The sequence details of these siRNAs are presented in the Table 1.

Finally, the selected siRNA and the lead formulation were validated in a pancreatic cancer cell line **(**Fig. 5**).** Here, LNP2 was used as a control formulation whose molar composition is reported in the literature and showed equivalent median effective dose (ED50) as the gold standard MC3-based Onpattro-like LNPs [24,27,46], CFPAC-1 cells were incubated with LNPs for 24 h. A decrease in pERK compared to total ERK was seen in a western blot analysis (Fig. 5**-A, B)**. Under similar treatment conditions, quantitative PCR showed a marked reduction in KRAS expression compared to the house-keeping beta-actin gene (Fig. 5**-C)**. Additionally, an MTT assay showed more efficient killing of CFPAC-1 cells when gemcitabine (10 nM) was used in combination with the siRNA treatment (LNP-2 or LNP-S3-tLyp-1 at 137 nM) at 24, 48, and 72 h **(**Fig. 5**-D)**. Also, these formulations were tested in an *in vivo* setting with the aim of developing a treatment strategy for KRAS-mutant cancers. The physicochemical characteristics and formulation details of the formulations tested in the *in vivo* studies are presented in Table 3.

3.5. In vivo biodistribution study: comparison of targeted and non-targeted LNPs in a pancreatic cancer model

As highlighted in the introduction, tLyp-1 is a potent targeting ligand for the NRP-1 receptor [38,39,66]. The effect of this targeting ligand on *in vivo* biodistribution was studied in the subcutaneous CFPAC-1 (human pancreatic cancer cell line) xenograft tumor model. The high expression of NRP-1 in pancreatic cancer cells, such as in the CFPAC-1 cell line, has been previously reported in the literature [67] and confirmed in this work by flowcytometry analysis (supplementary data - Fig. S7). The biodistribution of the selected nanoformulation, LNP-S3 functionalized with tLyp-1 and loaded with a fluorescent dye (DiR), was studied at 32 h post-injection (LNP-S3-tLyp-1-DiR) and it was compared with DiR-labelled LNP-S3 without a targeting ligand (LNP-S3-DiR). The results, illustrated in Fig. 6, show that the majority of both, the targeted and non-targeted LNPs, accumulated in the liver, a result that is in-line with the literature [26]. However, the tLyp1 functionalized LNPs showed significantly higher accumulation in the tumor, spleen, and lungs than the non-targeted ones. These organs also showed higher fluorescence signal per mg of tissue when using targeted LNPs (Fig. 6-B). These results highlight the importance of tLyp-1 as a targeting ligand in terms of enhancing the accumulation of siRNA-LNP in tumors expressing the neuropilin-1 (NRP-1) receptor.

3.6. In vivo toxicity studies: LNPs maximum tolerated dose in healthy mice

It is clear from the biodistribution study that only a fraction of the total injected dose reaches the tumor, while a significant amount of LNPs ends up in the liver and other organs. Therefore, it is important to determine not only the efficacy of these formulations but also their potential toxicity, especially as it relates to their accumulation in the liver. Regarding this, it is known that the potential toxicity of LNP could be attributed to the LNP components such as ionizable cationic lipid (ICL) [68–70]. In this study, two formulations containing two different amounts of C12–200 lipid where used, using a reference molar composition already reported (27). The formulations were adapted in the ratio of their components in order to keep constant the amount of siRNA dose, see Table 3, supplementary data - Fig. S9, and methods section for details. Hence, in this study, we determined the maximum tolerated dose for C12–200 based LNPs after 8 intravenous injections administered over a period of 4 weeks. Our results showed that one in four animals in the high dose group (LNP2-High) died a couple of days after the 8th injection, while the remaining mice exhibited poor health, and had to be euthanized, then their organs were collected for analysis. We saw extensive damage in the liver, spleen, and kidneys, as well as perturbations in some of the biochemical and hematological factors in the high-dose group (supplementary data - Fig. S10, S11, and S12). However, minimal adverse effects and no apparent change in the behavior of the mice were observed in the treatment group receiving the lower dose of C12–200 (LNP2-Low) (supplementary data - Fig. S10, S11, and S12). According to these results, the cumulative maximum tolerated dose for the intravenous administration of C12–200 based siRNA LNPs would be around 1.92 mg of total C12–200 per animal corresponding to about 64 mg/kg dose when calculated with an average body weight of 30 g per mouse. It should be noted that the *in vivo* toxicity assay was performed in healthy mouse model and that the toxicity of the LNPs could be aggravated in the pancreatic tumor model.

Previous studies reported no adverse events when intravenously administering a single bolus injection of C12–200 LNPs at a dose of 1 mg/kg of RNA, which would approximately equate to 7 to 10 mg/kg of C12–200 [48,71]. In another study, repeated administration of MC3-

LNPs have shown to cause minor liver damage when administered intravenously, twice a week for 2 weeks at a dose of 0.3 mg/kg of RNA cargo [68,72]. These studies did not test higher doses of ionizable lipid, since they were targeting liver which is the major organ of LNP accumulation. The median effective dose (ED50) for gene silencing in liver, with C12–200 or MC3 LNPs, were around 0.03 mg/kg RNA [27,46,48]. However, in our case, since only a fraction of the injected dose reaches the target tumor, we tested higher concentrations in-line with the dosing requirements for an *in vivo* efficacy study. In other safety studies with repeated injection of Stable Nucleic Acid Lipid Particles (SNALPs) which has a similar composition as MC3 LNPs, the maximum tolerated dose (MTD) in mice was reported to be 3 mg/kg in rats, while 12 mg/kg for mice [73]. The no observable adverse effect level (NOAEL) was reported to be around 1 mg/kg [73]. In summary, here we have demonstrated the safety of repeated dosing of C12–200 LNPs in a healthy mouse model at a higher dose than previously described. It appears that the C12–200 based LNPs could have a better safety profile than MC3-based LNPs.

3.7. In vivo efficacy study to compare the anti-cancer activity of targeted and non-targeted LNPs in combination with gemcitabine on a subcutaneous pancreatic cancer model – CFPAC-1

Once the biodistribution was analyzed and quantified, the next step was the evaluation of the *in vivo* antitumor response of the tLyp-1-functionalized LNP (prototype LNP-S3-tLyp-1) in comparison with that of the non-functionalized nanoformulation (LNP2), and that of the free drug. On the other hand, it is known that switching down specific targets, notably KRAS, might not be sufficient to elicit the adequate therapeutic response. Therefore, a combination of the nanoformulation plus gemcitabine, typically used to treat pancreatic cancer, was adopted in order to assess the value of the combination therapy. To this end, a subcutaneous human xenograft pancreatic cancer model was established in a nude mouse using a CFPAC-1 cell line. Once the tumor reached appropriate size (approximately 5 to 7 mm), mice were treated with gemcitabine alone (100 mg/kg) or gemcitabine in combination with anti-KRAS siRNA encapsulated in LNPs with or without the targeting ligand, Fig. 7**-A**. The results presented in Fig. 7**-B**, showing the tumor size evolution over the time, indicated that the size of the tumor, in the PBS control group grown until the end of the experiment and in the gemcitabine group (drug), remained stagnant. In contrast, the combination treatment with anti-KRAS siRNA, delivered with both targeted and non-targeted nanosystems, led to a drastic reduction of the tumor size. The statistical analysis for change in tumor volume is presented in the supplementary data, **Fig. S8-A** and indicated in the Fig. 7**-B**. The tumors collected from different treatments at the end of the study are presented in Fig. 7**-D.** This reduction was more remarkable when the treatment included the tLyp-1-functionalized LNPs. This enhanced therapeutic efficacy could be attributed to the enhanced accumulation of LNPs in the tumor in the presence of a targeting ligand as shown in Fig. 6. The survival plot is presented in Fig. 7**-C**. Most of the mice from the PBS (no treatment group) survived until the end of the experiment even though their tumor volume was larger, while some of the mice in the gemcitabine and gemcitabine + LNP treatment groups spontaneously died during the course of the study even though the tumor volume was reduced. Gemcitabine treatment group showed the lowest survival percentage (29%) compared to LNP-S3-tLyp-1 + Gemcitabine (43%), LNP-2 + Gemcitabine (57%), and untreated mice (71%) by the end of the treatment. Although the body weight of those mice that survived did not vary >20% of the initial body weight, **supplementary data – Fig. S8-B,** the experiment was stopped on day 10 as many mice died in the treatment groups. The rest of mice were sacrificed, and tumors collected for analysis on day 10. The low survival of the mice in the treatment groups could be attributed to the toxicity of gemcitabine. No additive effect of toxicity was seen in the groups receiving both gemcitabine and LNPs. More studies are needed to define a safe dose and dosing regimen for gemcitabine and the combination therapy with LNPs in our pancreatic cancer mouse model. Previous studies have shown the safety of gemcitabine administration between 60 and 120 mg/kg every three days for up to four I.P. injections in breast or pancreatic cancer mouse models [74,75]. Hence, the observed toxicity from gemcitabine was unexpected.

As a proof of *in vivo* siRNA delivery, tumors collected after the treatment showed significantly reduced KRAS expression in qPCR (Fig. 7**-E**), along with reduction in activation of pERK in an immunofluorescence assay (Fig. 7**-F**). Taken together these results, we concluded that silencing KRAS with siRNA-LNPs and *in vivo* downregulation of KRAS and pERK seems to enhance the therapeutic benefits of gemcitabine in a CFPAC-1 subcutaneous mouse model.

As of 2023, there are three LNP-based RNA drugs and vaccines approved in the clinic, and many more are being tested in clinical trials for various indications [22,24,76]. LNPs have proven to be one of the most efficient and clinically advanced delivery system for nucleic acids [22,24,76]. Currently, the applications are mainly limited to liver associated diseases, vaccines, and immunotherapy [22,24,76]. Efficient delivery to solid tumors and other extra-hepatic tissues is a major challenge that is yet to be concurred [22,24,76]. Years of previous research and an explosion of interest in LNPs following its success as a COVID-19 vaccine, will spark more discoveries making this delivery technology much safer, widen its application and improve its accessibility. Cancer is a challenging target, however deeper understanding of its biology, combining appropriate immune-modulating therapies along with other modalities could bring promising therapies for people in need. In this direction, ligand targeted LNPs could be leading a way to reach extra-hepatic targets, which makes this work highly relevant to current scenario.

4. Conclusions

This work highlights the importance of a rational design of both, the siRNA cargo and the carrier (LNPs) in the development of new siRNA-based therapies. It also highlights that, when targeting specific organs, other than the liver, the functionalization of the nanocarrier may be critical. Here, we found that small changes to the chemical modification of siRNA anti-KRAS drastically affect their functional efficacy. Through *in-vitro* screening, we identified promising siKRAS candidates (siKRAS-ESC+ and siKRAS-LNA) and loaded one of them (siKRAS-LNA) into a new composition of LNPs containing Tween® 80 and functionalized with the tumor-homing peptide (tLyp-1). This new targeted nanotherapy candidate exhibited a significant tumor accumulation and led to a significant reduction in the tumor size when combined with gemcitabine. These results clearly indicate that the application of siRNA based KRAS inhibition is a viable and promising strategy for developing a cancer treatment.

CRediT authorship contribution statement

Shubaash Anthiya: Conceptualization, Methodology, Investigation, Validation, Formal analysis, Writing – original draft, Writing – review & editing, Visualization. **Süleyman Can Öztürk:** Methodology, Investigation, Formal analysis, Visualization. **Hamdullah Yanik:** Investigation, Formal analysis, Visualization. **Ece Tavukcuoglu:** Investigation, Formal analysis, Visualization. **Adem Sahin:** Investigation, Formal analysis, Visualization. **Dhrubajyoti Datta:** Resources, Visualization, Writing – review & editing. **Klaus Charisse:** Resources. **David Moreira Álvarez:** Investigation. **Mabel Loza:** Supervision. **Alfonso Calvo:** Resources. **Einar Sulheim:** Investigation, Formal analysis, Writing – review & editing. **Simon Loevenich:** Investigation, Formal analysis. **Geir Klinkenberg:** Supervision. **Ruth Schmid:** Supervision, Writing – review & editing, Project administration. **Muthiah Manoharan:** Conceptualization, Methodology, Investigation, Validation, Writing – review & editing, Resources. **Güneş Esendağlı:** Supervision, Methodology, Validation. **Maria Jose Alonso:** Conceptualization, Methodology,

Validation, Writing – original draft, Writing – review & editing, Supervision, Project administration, Funding acquisition.

Declaration of Competing Interest

M.J.A. is a founder and shareholders of Libera Bio. S.A. is an employee of Sanofi Pasteur, France.

Data availability

Data will be made available on request.

Acknowledgments

This work was supported by the 2-INTRATARGET project (PCIN-2017-129/AEI) funded by MINECO-PCIN-2017-129/AEI, under the frame of EuroNanoMed III; by Consellería de Educación e Ordenación Universitaria, Xunta de Galicia's Grupos de referencia competitiva (grant number ED431C 2017/09). The authors thank TÜBİTAK (The Scientific and Technical Research Council of Turkey) for supporting this project (Project number : 217S068). S.A acknowledges the financial support for his postdoctoral research by the 2-INTRATARGET project (PCIN-2017-129/AEI) funded by MINECO-PCIN-2017- 129/AEI, under the frame of EuroNanoMed III. The authors thank Fernando Torres Andon for critical reading of the manuscript. The authors express their sincere gratitude to Catarina Afonso, Belen Cuesta, Balbina Fernandez, Lucia Alvariño, Ana Senra, Jose Malagon (CEBEGA, USC), Anxo Vidal (CIMUS) for their invaluable technical support and discussion.

Appendix A. Supplementary data

Supplementary data to this article can be found online at https://doi.org/10.1016/j.jconrel.2023.03.016.

References

[1] T.L. Yuan, C. Fellmann, C.-S. Lee, C.D. Ritchie, V. Thapar, L.C. Lee, D.J. Hsu, D. Grace, J.O. Carver, J. Zuber, J. Luo, F. McCormick, S.W. Lowe, Development of siRNA payloads to target KRAS -mutant cancer, Cancer Discov. 4 (2014) 1182–1197, https://doi.org/10.1158/2159-8290.CD-13-0900.

[2] P. Liu, Y. Wang, X. Li, Targeting the untargetable KRAS in cancer therapy, Acta Pharm. Sin. B 9 (2019) 871–879, https://doi.org/10.1016/j.apsb.2019.03.002.

[3] I. Ferrer, J. Zugazagoitia, S. Herbertz, W. John, L. Paz-Ares, G. Schmid-Bindert, KRAS-mutant non-small cell lung cancer: from biology to therapy, Lung Cancer 124 (2018) 53–64, https://doi.org/10.1016/j.lungcan.2018.07.013.

[4] E. Zorde Khvalevsky, R. Gabai, I.H. Rachmut, E. Horwitz, Z. Brunschwig, A. Orbach, A. Shemi, T. Golan, A.J. Domb, E. Yavin, H. Giladi, L. Rivkin, A. Simerzin, R. Eliakim, A. Khalaileh, A. Hubert, M. Lahav, Y. Kopelman, E. Goldin, A. Dancour, Y. Hants, S. Arbel-Alon, R. Abramovitch, A. Shemi, E. Galun, Mutant KRAS is a druggable target for pancreatic cancer, Proc. Natl. Acad. Sci. 110 (2013) 20723–20728, https://doi.org/10.1073/pnas.1314307110.

[5] J.B. Fleming, G.L. Shen, S.E. Holloway, M. Davis, R.A. Brekken, Molecular consequences of silencing mutant K-ras in pancreatic cancer cells: justification for K-ras-directed therapy, Mol. Cancer Res. 3 (2005) 413–423, https://doi.org/10.1158/1541-7786.MCR-04-0206.

[6] S. Réjiba, S. Wack, M. Aprahamian, A. Hajri, K-ras oncogene silencing strategy reduces tumor growth and enhances gemcitabine chemotherapy efficacy for pancreatic cancer treatment, Cancer Sci. 98 (2007) 1128–1136, https://doi.org/10.1111/j.1349-7006.2007.00506.x.

[7] N. Sunaga, D.S. Shames, L. Girard, M. Peyton, J.E. Larsen, H. Imai, J. Soh, M. Sato, N. Yanagitani, K. Kaira, Y. Xie, A.F. Gazdar, M. Mori, J.D. Minna, Knockdown of oncogenic KRAS in non–small cell lung cancers suppresses tumor growth and sensitizes tumor cells to targeted therapy, Mol. Cancer Ther. 10 (2011) 336–346, https://doi.org/10.1158/1535-7163.MCT-10-0750.

[8] Y. Ramot, S. Rotkopf, R.M. Gabai, E. Zorde Khvalevsky, S. Muravnik, G.A. Marzoli, A.J. Domb, A. Shemi, A. Nyska, Preclinical safety evaluation in rats of a polymeric matrix containing an siRNA drug used as a local and prolonged delivery system for pancreatic Cancer therapy, Toxicol. Pathol. 44 (2016) 856–865, https://doi.org/10.1177/0192623316645860.

[9] T. Golan, E.Z. Khvalevsky, A. Hubert, R.M. Gabai, N. Hen, A. Segal, A. Domb, G. Harari, E. Ben David, S. Raskin, Y. Goldes, E. Goldin, R. Eliakim, M. Lahav, Y. Kopleman, A. Dancour, A. Shemi, E. Galun, RNAi therapy targeting KRAS in combination with chemotherapy for locally advanced pancreatic cancer patients, Oncotarget. 6 (2015) 24560–24570, https://doi.org/10.18632/oncotarget.4183.

[10] S. Kamerkar, V.S. LeBleu, H. Sugimoto, S. Yang, C.F. Ruivo, S.A. Melo, J.J. Lee, R. Kalluri, Exosomes facilitate therapeutic targeting of oncogenic KRAS in pancreatic cancer, Nature. 546 (2017) 498–503, https://doi.org/10.1038/nature22341.

[11] A. Mehta, E. Dalle Vedove, L. Isert, O.M. Merkel, Targeting KRAS mutant lung Cancer cells with siRNA-loaded bovine serum albumin nanoparticles, Pharm. Res. 36 (2019) 133, https://doi.org/10.1007/s11095-019-2665-9.

[12] Y. Pei, L. Chen, Y. Huang, J. Wang, J. Feng, M. Xu, Y. Chen, Q. Song, G. Jiang, X. Gu, Q. Zhang, X. Gao, J. Chen, Sequential targeting TGF-β signaling and KRAS mutation increases therapeutic efficacy in pancreatic Cancer, Small. 15 (2019) 1900631, https://doi.org/10.1002/smll.201900631.

[13] M. Acunzo, G. Romano, G. Nigita, D. Veneziano, L. Fattore, A. Laganà, N. Zanesi, P. Fadda, M. Fassan, L. Rizzotto, R. Kladney, V. Coppola, C.M. Croce, Selective targeting of point-mutated KRAS through artificial microRNAs, Proc. Natl. Acad. Sci. 114 (2017) E4203–E4212, https://doi.org/10.1073/pnas.1620562114.

[14] W. Xue, J.E. Dahlman, T. Tammela, O.F. Khan, S. Sood, A. Dave, W. Cai, L. M. Chirino, G.R. Yang, R. Bronson, D.G. Crowley, G. Sahay, A. Schroeder, R. Langer, D.G. Anderson, T. Jacks, Small RNA combination therapy for lung cancer, Proc. Natl. Acad. Sci. 111 (2014) E3553–E3561, https://doi.org/10.1073/pnas.1412686111.

[15] L. Gu, Z.J. Deng, S. Roy, P.T. Hammond, A combination RNAi-Chemotherapy layer-by-layer nanoparticle for systemic targeting of KRAS/P53 with cisplatin to treat non–small cell lung cancer, Clin. Cancer Res. 23 (2017) 7312–7323, https://doi.org/10.1158/1078-0432.CCR-16-2186.

[16] K. Werner, F. Lademann, M.-L. Thepkaysone, B. Jahnke, D.E. Aust, C. Kahlert, G. Weber, J. Weitz, R. Grützmann, C. Pilarsky, Simultaneous gene silencing of KRAS and anti-apoptotic genes as a multitarget therapy, Oncotarget. 7 (2016) 3984–3992, https://doi.org/10.18632/oncotarget.6766.

[17] M.S. Strand, B.A. Krasnick, H. Pan, X. Zhang, Y. Bi, C. Brooks, C. Wetzel, N. Sankpal, T. Fleming, S.P. Goedegebuure, D.G. DeNardo, W.E. Gillanders, W. G. Hawkins, S.A. Wickline, R.C. Fields, Precision delivery of RAS-inhibiting siRNA to KRAS driven cancer via peptide-based nanoparticles, Oncotarget. 10 (2019) 4761–4775, https://doi.org/10.18632/oncotarget.27109.

[18] Y. Zhou, H. Wen, L. Gu, J. Fu, J. Guo, L. Du, X. Zhou, X. Yu, Y. Huang, H. Wang, Aminoglucose-functionalized, redox-responsive polymer nanomicelles for overcoming chemoresistance in lung cancer cells, J. Nanobiotechnol. 15 (2017) 1–17, https://doi.org/10.1186/s12951-017-0316-z.

[19] S.J. Ross, A.S. Revenko, L.L. Hanson, R. Ellston, A. Staniszewska, N. Whalley, S. K. Pandey, M. Revill, C. Rooney, L.K. Buckett, S.K. Klein, K. Hudson, B.P. Monia, M. Zinda, D.C. Blakey, P.D. Lyne, A.R. Macleod, Targeting KRAS-dependent tumors with AZD4785, a high-affinity therapeutic antisense oligonucleotide inhibitor of KRAS, Sci. Transl. Med. 9 (2017) eaal5253, https://doi.org/10.1126/scitranslmed.aal5253.

[20] B.M.D.C. Godinho, A. Khvorova, The era of RNA interference medicines: the clinical landscape of synthetic gene silencing drugs, Saúde Tecnol. (2020) 5–17, https://doi.org/10.25758/set.2227.

[21] T.C. Roberts, R. Langer, M.J.A. Wood, Advances in oligonucleotide drug delivery, Nat. Rev. Drug Discov. 19 (2020) 673–694, https://doi.org/10.1038/s41573-020-0075-7.

[22] E. Samaridou, J. Heyes, P. Lutwyche, Lipid nanoparticles for nucleic acid delivery: current perspectives, Adv. Drug Deliv. Rev. 154–155 (2020) 37–63, https://doi.org/10.1016/j.addr.2020.06.002.

[23] A. Shemi, E.Z. Khvalevsky, R.M. Gabai, A. Domb, Y. Barenholz, Multistep, effective drug distribution within solid tumors, Oncotarget. 6 (2015) 39564–39577, https://doi.org/10.18632/oncotarget.5051.

[24] A. Akinc, M.A. Maier, M. Manoharan, K. Fitzgerald, M. Jayaraman, S. Barros, S. Ansell, X. Du, M.J. Hope, T.D. Madden, B.L. Mui, S.C. Semple, Y.K. Tam, M. Ciufolini, D. Witzigmann, J.A. Kulkarni, R. van der Meel, P.R. Cullis, The Onpattro story and the clinical translation of nanomedicines containing nucleic acid-based drugs, Nat. Nanotechnol. 14 (2019) 1084–1087, https://doi.org/10.1038/s41565-019-0591-y.

[25] L. Schoenmaker, D. Witzigmann, J.A. Kulkarni, R. Verbeke, G. Kersten, W. Jiskoot, D.J.A. Crommelin, mRNA-lipid nanoparticle COVID-19 vaccines: structure and stability, Int. J. Pharm. 601 (2021), 120586, https://doi.org/10.1016/j.ijpharm.2021.120586.

[26] R. Zhang, R. El-Mayta, T.J. Murdoch, C.C. Warzecha, M.M. Billingsley, S. J. Shepherd, N. Gong, L. Wang, J.M. Wilson, D. Lee, M.J. Mitchell, Helper lipid structure influences protein adsorption and delivery of lipid nanoparticles to spleen and liver, Biomater. Sci. 9 (2021) 1449–1463, https://doi.org/10.1039/d0bm01609h.

[27] K.J. Kauffman, J.R. Dorkin, J.H. Yang, M.W. Heartlein, F. Derosa, F.F. Mir, O. S. Fenton, D.G. Anderson, Optimization of lipid nanoparticle formulations for mRNA delivery in vivo with fractional factorial and definitive screening designs, Nano Lett. 15 (2015) 7300–7306, https://doi.org/10.1021/acs.nanolett.5b02497.

[28] Y. Dong, K.T. Love, J.R. Dorkin, S. Sirirungruang, Y. Zhang, D. Chen, R.L. Bogorad, H. Yin, Y. Chen, A.J. Vegas, C.A. Alabi, G. Sahay, K.T. Olejnik, W. Wang, A. Schroeder, A.K.R. Lytton-Jean, D.J. Siegwart, A. Akinc, C. Barnes, S.A. Barros, M. Carioto, K. Fitzgerald, J. Hettinger, V. Kumar, T.I. Novobrantseva, J. Qin, W. Querbes, V. Koteliansky, R. Langer, D.G. Anderson, Lipopeptide nanoparticles for potent and selective siRNA delivery in rodents and nonhuman primates, Proc. Natl. Acad. Sci. 111 (2014) 3955–3960, https://doi.org/10.1073/pnas.1322937111.

[29] J.A. Kulkarni, D. Witzigmann, J. Leung, Y.Y.C. Tam, P.R. Cullis, On the role of helper lipids in lipid nanoparticle formulations of siRNA, Nanoscale. 11 (2019) 21733–21739, https://doi.org/10.1039/C9NR09347H.

[30] Q. Cheng, T. Wei, L. Farbiak, L.T. Johnson, S.A. Dilliard, D.J. Siegwart, Selective organ targeting (SORT) nanoparticles for tissue-specific mRNA delivery and CRISPR–Cas gene editing, Nat. Nanotechnol. 15 (2020) 313–320, https://doi.org/10.1038/s41565-020-0669-6.
[31] S.A. Dilliard, Q. Cheng, D.J. Siegwart, On the mechanism of tissue-specific mRNA delivery by selective organ targeting nanoparticles, Proc. Natl. Acad. Sci. 118 (2021) 1–14, https://doi.org/10.1073/pnas.2109256118.
[32] R.C. Ryals, S. Patel, C. Acosta, M. McKinney, M.E. Pennesi, G. Sahay, The effects of PEGylation on LNP based mRNA delivery to the eye, PLoS One 15 (2020) 1–17, https://doi.org/10.1371/journal.pone.0241006.
[33] L.M. Kranz, M. Diken, H. Haas, S. Kreiter, C. Loquai, K.C. Reuter, M. Meng, D. Fritz, F. Vascotto, H. Hefesha, C. Grunwitz, M. Vormehr, Y. Hüsemann, A. Selmi, A. N. Kuhn, J. Buck, E. Derhovanessian, R. Rae, S. Attig, J. Diekmann, R. A. Jabulowsky, S. Heesch, J. Hassel, P. Langguth, S. Grabbe, C. Huber, Ö. Türeci, U. Sahin, Systemic RNA delivery to dendritic cells exploits antiviral defence for cancer immunotherapy, Nature. 534 (2016) 396–401, https://doi.org/10.1038/nature18300.
[34] Y.Y.C. Tam, S. Chen, J. Zaifman, Y.K. Tam, P.J.C. Lin, S. Ansell, M. Roberge, M. A. Ciufolini, P.R. Cullis, Small molecule ligands for enhanced intracellular delivery of lipid nanoparticle formulations of siRNA, Nanomedicine 9 (2013) 665–674, https://doi.org/10.1016/j.nano.2012.11.006.
[35] A. Tam, J. Kulkarni, K. An, L. Li, D. Dorscheid, G. Singhera, P. Bernatchez, G. Reid, K. Chan, D. Witzigmann, P. Cullis, D. Sin, C. Lim, Lipid nanoparticle formulations for optimal RNA-based topical delivery to murine airways, Eur. J. Pharm. Sci. 176 (2022), 106234, https://doi.org/10.1016/j.ejps.2022.106234.
[36] N.R.M. Saunders, M.S. Paolini, O.S. Fenton, L. Poul, J. Devalliere, F. Mpambani, A. Darmon, M. Bergère, O. Jibault, M. Germain, R. Langer, A Nanoprimer to improve the systemic delivery of siRNA and mRNA, Nano Lett. 20 (2020) 4264–4269, https://doi.org/10.1021/acs.nanolett.0c00752.
[37] B. Ouyang, W. Poon, Y.-N. Zhang, Z.P. Lin, B.R. Kingston, A.J. Tavares, Y. Zhang, J. Chen, M.S. Valic, A.M. Syed, P. MacMillan, J. Couture-Senécal, G. Zheng, W.C. W. Chan, The dose threshold for nanoparticle tumour delivery, Nat. Mater. 19 (2020) 1362–1371, https://doi.org/10.1038/s41563-020-0755-z.
[38] L. Roth, L. Agemy, V.R. Kotamraju, G. Braun, T. Teesalu, K.N. Sugahara, J. Hamzah, E. Ruoslahti, Transtumoral targeting enabled by a novel neuropilin-binding peptide, Oncogene. 31 (2012) 3754–3763, https://doi.org/10.1038/onc.2011.537.
[39] C. Teijeiro-Valiño, R. Novoa-Carballal, E. Borrajo, A. Vidal, M. Alonso-Nocelo, M. de la Fuente Freire, P.P. Lopez-Casas, M. Hidalgo, N. Csaba, M.J. Alonso, A multifunctional drug nanocarrier for efficient anticancer therapy, J. Control. Release 294 (2019) 154–164, https://doi.org/10.1016/j.jconrel.2018.12.002.
[40] W. Ou, R.K. Thapa, L. Jiang, Z.C. Soe, M. Gautam, J.-H. Chang, J.-H. Jeong, S. K. Ku, H.-G. Choi, C.S. Yong, J.O. Kim, Regulatory T cell-targeted hybrid nanoparticles combined with immuno-checkpoint blockage for cancer immunotherapy, J. Control. Release 281 (2018) 84–96, https://doi.org/10.1016/j.jconrel.2018.05.018.
[41] S. Singh, H. Singh, A. Tuknait, K. Chaudhary, B. Singh, S. Kumaran, G.P. S. Raghava, PEPstrMOD: structure prediction of peptides containing natural, non-natural and modified residues, Biol. Direct 10 (2015) 73, https://doi.org/10.1186/s13062-015-0103-4.
[42] J.B. Lee, K. Zhang, Y.Y.C. Tam, Y.K. Tam, N.M. Belliveau, V.Y.C. Sung, P.J.C. Lin, E. LeBlanc, M.A. Ciufolini, P.S. Rennie, P.R. Cullis, Lipid nanoparticle siRNA systems for silencing the androgen receptor in human prostate cancer in vivo, Int. J. Cancer 131 (2012) E781–E790, https://doi.org/10.1002/ijc.27361.
[43] J. Schindelin, I. Arganda-Carreras, E. Frise, V. Kaynig, M. Longair, T. Pietzsch, S. Preibisch, C. Rueden, S. Saalfeld, B. Schmid, J.-Y. Tinevez, D.J. White, V. Hartenstein, K. Eliceiri, P. Tomancak, A. Cardona, Fiji: an open-source platform for biological-image analysis, Nat. Methods 9 (2012) 676–682, https://doi.org/10.1038/nmeth.2019.
[44] D.P. Ivanov, A.M. Grabowska, M.C. Garnett, High-Throughput Spheroid Screens Using Volume, Resazurin Reduction, and Acid Phosphatase Activity, 2017, pp. 43–59, https://doi.org/10.1007/978-1-4939-6960-9_4.
[45] P.H. Sugarbaker, O.A. Stuart, Intraperitoneal gemcitabine chemotherapy is safe for patients with resected pancreatic cancer: final clinical and pharmacologic data from a phase II protocol and recommended future directions, J. Gastrointest. Oncol. 12 (2021) S99–S109, https://doi.org/10.21037/jgo-2020-02.
[46] M. Jayaraman, S.M. Ansell, B.L. Mui, Y.K. Tam, J. Chen, X. Du, D. Butler, L. Eltepu, S. Matsuda, J.K. Narayanannair, K.G. Rajeev, I.M. Hafez, A. Akinc, M.A. Maier, M. A. Tracy, P.R. Cullis, T.D. Madden, M. Manoharan, M.J. Hope, Maximizing the potency of siRNA lipid nanoparticles for hepatic gene silencing in vivo**, Angew. Chem. Int. Ed. 51 (2012) 8529–8533, https://doi.org/10.1002/anie.201203263.
[47] K.J. Hassett, K.E. Benenato, E. Jacquinet, A. Lee, A. Woods, O. Yuzhakov, S. Himansu, J. Deterling, B.M. Geilich, T. Ketova, C. Mihai, A. Lynn, I. McFadyen, M.J. Moore, J.J. Senn, M.G. Stanton, Ö. Almarsson, G. Ciaramella, L.A. Brito, Optimization of lipid nanoparticles for intramuscular administration of mRNA vaccines, Mol. Ther. - Nucleic Acids. 15 (2019) 1–11, https://doi.org/10.1016/j.omtn.2019.01.013.
[48] K.T. Love, K.P. Mahon, C.G. Levins, K.A. Whitehead, W. Querbes, J.R. Dorkin, J. Qin, W. Cantley, L.L. Qin, T. Racie, M. Frank-Kamenetsky, K.N. Yip, R. Alvarez, D.W.Y.Y. Sah, A. de Fougerolles, K. Fitzgerald, V. Koteliansky, A. Akinc, R. Langer, D.G. Anderson, Lipid-like materials for low-dose, in vivo gene silencing, Proc. Natl. Acad. Sci. 107 (2010) 1864–1869, https://doi.org/10.1073/pnas.0910603106.
[49] R. Leventis, J.R. Silvius, Interactions of mammalian cells with lipid dispersions containing novel metabolizable cationic amphiphiles, BBA - Biomembr. 1023 (1990) 124–132, https://doi.org/10.1016/0005-2736(90)90017-I.
[50] L. Stamatatos, R. Leventis, M.J. Zuckermann, J.R. Silvius, Interactions of cationic lipid vesicles with negatively charged phospholipid vesicles and biological membranes, Biochemistry. 27 (1988) 3917–3925, https://doi.org/10.1021/bi00411a005.
[51] B. Pitard, D. Habrant, Supramolecular gene transfection agents, in: Compr. Supramol. Chem. II. Second Edi, Elsevier, 2017, pp. 365–389, https://doi.org/10.1016/B978-0-12-409547-2.12563-6.
[52] K. Crook, B.J. Stevenson, M. Dubouchet, D.J. Porteous, Inclusion of cholesterol in DOTAP transfection complexes increases the delivery of DNA to cells in vitro in the presence of serum, Gene Ther. 5 (1998) 137–143, https://doi.org/10.1038/sj.gt.3300554.
[53] T.W. Kim, Y.J. Kim, H. Chung, I.C. Kwon, H.C. Sung, S.Y. Jeong, The role of non-ionic surfactants on cationic lipid mediated gene transfer, J. Control. Release 82 (2002) 455–465, https://doi.org/10.1016/S0168-3659(02)00138-4.
[54] C. Lu, D.J. Stewart, J.J. Lee, L. Ji, R. Ramesh, G. Jayachandran, M.I. Nunez, I. I. Wistuba, J.J. Erasmus, M.E. Hicks, E.A. Grimm, J.M. Reuben, V. Baladandayuthapani, N.S. Templeton, J.D. McMannis, J.A. Roth, Phase I clinical trial of systemically administered TUSC2(FUS1)-nanoparticles mediating functional gene transfer in humans, PLoS One 7 (2012), e34833, https://doi.org/10.1371/journal.pone.0034833.
[55] A. Peletta, E. Prompetchara, K. Tharakhet, P. Kaewpang, S. Buranapraditkun, T. Techawiwattanaboon, T. Jbilou, P. Krangvichian, S. Sirivichayakul, S. Manopwisedjaroen, A. Thitithanyanont, K. Patarakul, K. Ruxrungtham, C. Ketloy, G. Borchard, Dna vaccine administered by cationic lipoplexes or by in vivo electroporation induces comparable antibody responses against sars-cov-2 in mice, Vaccines. 9 (2021), https://doi.org/10.3390/vaccines9080874.
[56] R. Verbeke, I. Lentacker, L. Wayteck, K. Breckpot, M. Van Bockstal, B. Descamps, C. Vanhove, S.C. De Smedt, H. Dewitte, Co-delivery of nucleoside-modified mRNA and TLR agonists for cancer immunotherapy: restoring the immunogenicity of immunosilent mRNA, J. Control. Release 266 (2017) 287–300, https://doi.org/10.1016/j.jconrel.2017.09.041.
[57] M.J. Carrasco, S. Alishetty, M.G. Alameh, H. Said, L. Wright, M. Paige, O. Soliman, D. Weissman, T.E. Cleveland, A. Grishaev, M.D. Buschmann, Ionization and structural properties of mRNA lipid nanoparticles influence expression in intramuscular and intravascular administration, Commun. Biol. 4 (2021) 1–15, https://doi.org/10.1038/s42003-021-02441-2.
[58] P. Patel, N.M. Ibrahim, K. Cheng, The importance of apparent pKa in the development of nanoparticles encapsulating siRNA and mRNA, Trends Pharmacol. Sci. 42 (2021) 448–460, https://doi.org/10.1016/j.tips.2021.03.002.
[59] J.R. Melamed, K.A. Hajj, N. Chaudhary, D. Strelkova, M.L. Arral, N. Pardi, M.-G. Alameh, J.B. Miller, L. Farbiak, D.J. Siegwart, D. Weissman, K.A. Whitehead, Lipid nanoparticle chemistry determines how nucleoside base modifications alter mRNA delivery, J. Control. Release 341 (2022) 206–214, https://doi.org/10.1016/j.jconrel.2021.11.022.
[60] B.L. Mui, Y.K. Tam, M. Jayaraman, S.M. Ansell, X. Du, Y.Y.C. Tam, P.J. Lin, S. Chen, J.K. Narayanannair, K.G. Rajeev, M. Manoharan, A. Akinc, M.A. Maier, P. Cullis, T.D. Madden, M.J. Hope, Influence of polyethylene glycol lipid desorption rates on pharmacokinetics and pharmacodynamics of siRNA lipid nanoparticles, Mol. Ther. - Nucleic Acids. 2 (2013), e139, https://doi.org/10.1038/mtna.2013.66.
[61] E. Gasteiger, C. Hoogland, A. Gattiker, S. Duvaud, M.R. Wilkins, R.D. Appel, A. Bairoch, Protein Identification and Analysis Tools on the ExPASy Server, Humana Press, Totowa, NJ, 2005, https://doi.org/10.1385/1592598900.
[62] E. Chargaff, The protamine salts of phosphatides, with remarks on the problem of lipoproteins, J. Biol. Chem. 125 (1938) 661–670, https://doi.org/10.1016/s0021-9258(18)73958-6.
[63] P. Kaczmarek, W. Szczepanik, M. Jeżowska-Bojczuk, Acid–base, coordination and oxidative properties of systems containing ATP, l-histidine and Ni(ii) ions, Dalton Trans. (2005) 3653, https://doi.org/10.1039/b508962j.
[64] G. Sahay, W. Querbes, C. Alabi, A. Eltoukhy, S. Sarkar, C. Zurenko, E. Karagiannis, K. Love, D. Chen, R. Zoncu, Y. Buganim, A. Schroeder, R. Langer, D.G. Anderson, Efficiency of siRNA delivery by lipid nanoparticles is limited by endocytic recycling, Nat. Biotechnol. 31 (2013) 653–658, https://doi.org/10.1038/nbt.2614.
[65] J. Gilleron, W. Querbes, A. Zeigerer, A. Borodovsky, G. Marsico, U. Schubert, K. Manygoats, S. Seifert, C. Andree, M. Stöter, H. Epstein-Barash, L. Zhang, V. Koteliansky, K. Fitzgerald, E. Fava, M. Bickle, Y. Kalaidzidis, A. Akinc, M. Maier, M. Zerial, Image-based analysis of lipid nanoparticle-mediated siRNA delivery, intracellular trafficking and endosomal escape, Nat. Biotechnol. 31 (2013) 638–646, https://doi.org/10.1038/nbt.2612.
[66] A. Ayo, P. Laakkonen, Peptide-based strategies for targeted tumor treatment and imaging, 2021, https://doi.org/10.3390/pharmaceutics13040481.
[67] L.H. He, Y.L. He, W.H. Zuo, Y. Kang, H. Xue, L.Y. Wang, Y.L. Zhang, Y. Meng, Neuropilin1 silencing impairs the proliferation and migration of cells in pancreatic cancer, J. Clin. Lab. Anal. 34 (2020) 1–7, https://doi.org/10.1002/jcla.23394.
[68] M. Sedic, J.J. Senn, A. Lynn, M. Laska, M. Smith, S.J. Platz, J. Bolen, S. Hoge, A. Bulychev, E. Jacquinet, V. Bartlett, P.F. Smith, Safety evaluation of lipid nanoparticle–formulated modified mRNA in the Sprague-Dawley Rat and Cynomolgus Monkey, Vet. Pathol. 55 (2018) 341–354, https://doi.org/10.1177/0300985817738095.
[69] A.Y. AlBaloul, Y. Sato, N. Maishi, K. Hida, H. Harashima, Two modes of toxicity of lipid nanoparticles containing a pH-sensitive cationic lipid on human A375 and A375-SM melanoma cell lines, BPB Rep. 2 (2019) 48–55, https://doi.org/10.1248/bpbreports.2.4_48.
[70] J. Christensen, K. Litherland, T. Faller, E. Van De Kerkhof, F. Natt, J. Hunziker, J. Boos, I. Beuvink, K. Bowman, J. Baryza, M. Beverly, C. Vargeese, O. Heudi, M. Stoeckli, J. Krauser, P. Swart, Biodistribution and metabolism studies of lipid

nanoparticle- formulated internally [3H]-labeled siRNA in Mices, Drug Metab. Dispos. 42 (2014) 431–440, https://doi.org/10.1124/dmd.113.055434.
[71] F. DeRosa, B. Guild, S. Karve, L. Smith, K. Love, J.R. Dorkin, K.J. Kauffman, J. Zhang, B. Yahalom, D.G. Anderson, M.W. Heartlein, Therapeutic efficacy in a hemophilia B model using a biosynthetic mRNA liver depot system, Gene Ther. 23 (2016) 699–707, https://doi.org/10.1038/gt.2016.46.
[72] T. Coelho, D. Adams, A. Silva, P. Lozeron, P.N. Hawkins, T. Mant, J. Perez, J. Chiesa, S. Warrington, E. Tranter, M. Munisamy, R. Falzone, J. Harrop, J. Cehelsky, B.R. Bettencourt, M. Geissler, J.S. Butler, A. Sehgal, R.E. Meyers, Q. Chen, T. Borland, R.M. Hutabarat, V.A. Clausen, R. Alvarez, K. Fitzgerald, C. Gamba-Vitalo, S.V. Nochur, A.K. Vaishnaw, D.W.Y. Sah, J.A. Gollob, O.B. Suhr, Safety and efficacy of RNAi therapy for transthyretin amyloidosis, N. Engl. J. Med. 369 (2013) 819–829, https://doi.org/10.1056/nejmoa1208760.
[73] S.A. Barros, J.A. Gollob, Safety profile of RNAi nanomedicines, Adv. Drug Deliv. Rev. 64 (2012) 1730–1737, https://doi.org/10.1016/j.addr.2012.06.007.
[74] A. Cividalli, F. Mauro, E. Livdi, F. Ceciarelli, P. Altavista, G. Cruciani, D. Tirindelli Danesi, Schedule dependent toxicity and efficacy of combined gemcitabine/paclitaxel treatment in mouse adenocarcinoma, J. Cancer Res. Clin. Oncol. 126 (2000) 461–467, https://doi.org/10.1007/PL00021282.
[75] K. Öztürk, G. Esendağlı, M.U. Gürbüz, M. Tülü, S. Çalış, Effective targeting of gemcitabine to pancreatic cancer through PEG-cored Flt-1 antibody-conjugated dendrimers, Int. J. Pharm. 517 (2017) 157–167, https://doi.org/10.1016/j.ijpharm.2016.12.009.
[76] X. Huang, N. Kong, X. Zhang, Y. Cao, R. Langer, W. Tao, The landscape of mRNA nanomedicine, Nat. Med. 28 (2022) 2273–2287, https://doi.org/10.1038/s41591-022-02061-1.